

# Two-electron lateral quantum-dot molecules in a magnetic field

M. Helle,\* A. Harju, and R. M. Nieminen

*Laboratory of Physics, Helsinki University of Technology, P. O. Box 1100 FIN-02015 HUT, Finland*

(Dated: September 26, 2018)

Laterally coupled quantum dot molecules are studied using exact diagonalization techniques. We examine the two-electron singlet-triplet energy difference as a function of magnetic field strength and investigate the magnetization and vortex formation of two- and four-minima lateral quantum dot molecules. Special attention is paid to the analysis of how the distorted symmetry affects the properties of quantum-dot molecules.

PACS numbers: 73.21.La,73.22.-f,75.75.+a,73.21.-b

## I. INTRODUCTION

The crossover from two-dimensional electron systems (2DES) to meso- and nanoscale quantum dots (QDs) is an interesting subject. In the infinite quantum Hall systems the actual arrangement of impurities or disorder does not play a role, even if the presence of disorder-induced localized states is vital for the Hall plateaus to occur.<sup>1</sup> In the few-electron QDs, the type of disorder is certainly an important issue. In the past, the majority of studies have concentrated on highly symmetric parabolic QDs without disorder. The rich spectrum of crossing energy levels as a function of magnetic field and strong interaction effects are nowadays rather well characterized for the cases with a symmetric confinement potential.<sup>2</sup> Recently, the focus has turned to understanding properties of QDs in less symmetric confinement potentials. For example, the rather simple far-infrared excitation spectrum of a purely parabolic QD is nowadays well understood,<sup>3</sup> whereas the lowered symmetry introduces new features in the spectrum whose interpretation is not straightforward at all.<sup>4,5,6,7,8,9,10,11</sup> Moreover, the lowered symmetry also gives rise to modified ground state properties such as level anticrossings and altered spin-phase diagram as a function of magnetic field.<sup>12,13</sup>

After Loss and DiVincenzo proposition,<sup>14</sup> coupled quantum dots have gained interest due to possible realization as spin-qubit based quantum gates in quantum computing.<sup>15,16,17</sup> In addition to coherent single-spin operations, the two-spin operations are sufficient for assembling any quantum computation. Recent experiments have shown a remarkable success in characterizing the few-electron eigenlevels,<sup>18,19,20</sup> approximating relaxation and time-averaged coherence times and mechanisms,<sup>21,22</sup> and reading single-spin or two-spin states<sup>23,24</sup> of the QDs whereas the coherent manipulation of spin systems remained out of reach until very recent measurements on two-spin rotations.<sup>25</sup>

In this paper we concentrate on two-electron quantum dot molecules. These molecules consist of laterally, closely coupled quantum dots. We treat correlation effects between the electrons properly by directly diagonalizing the Hamiltonian matrix in the many-body basis (exact diagonalization technique). This allows direct

access to the ground state energy levels and all excited states for both spin-singlet and spin-triplet states. We study these levels as well as singlet-triplet splitting and magnetizations as a function of magnetic field and dot-dot separation. We also analyze the properties of many-body wave functions in detail.

The magnetic field dependence of the ground state energy and singlet-triplet splitting in non-parabolic QDs have attracted recent interest.<sup>12,13,18,26,27,28,29,30,31,32,33</sup> Magnetizations in QDs have been measured indirectly with transport measurements<sup>34</sup> and recently with a direct technique with improved sensitivity.<sup>35</sup> For both measurements, semi-classical approaches cannot explain the results. Also the magnetizations of nanoscale QDs do not show non-equilibrium currents and de Haas-van Alphen oscillations which are observed in 2DES and mesoscopic QDs.<sup>36</sup> In the nanoscale QDs the quantum confinement and Coulomb interactions modify the system compared to the 2DES.<sup>35</sup> Theoretically, magnetization (at zero temperature) is straightforward to calculate as the derivative of the total energy with respect to magnetic field. Magnetizations have been calculated for a small number of electrons in a parabolic QD,<sup>37</sup> in a square dot with a repulsive impurity,<sup>38</sup> as well as for anisotropic QDs,<sup>27</sup> and for self-assembled QDs and quantum rings.<sup>39</sup> The magnetization curves have been calculated using density-functional theory for rectangular QDs<sup>26</sup> and using the Hartree approximation for other types of non-circular QDs.<sup>40</sup> A tight-binding model for 10-100 electrons in a single or two coupled QDs has been used to calculate magnetization curves.<sup>41</sup>

Calculations of vortices in QDs have also attracted much interest lately.<sup>42,43,44,45,46</sup> Even if the vortices are not directly experimentally observable, they reveal interesting properties of electron-electron correlations and of the structure of the wave function. The nucleation of vortices in QD systems could perhaps be observed by measuring magnetizations, where each peak would correspond to one vortex added in the system. However, the magnetization is difficult to measure for a small number of electrons, especially with direct methods. Moreover, in a non-circular symmetry, as in quantum dot molecules, and at high magnetic field strengths the magnetization curves may become more complicated.

In our previous studies we have examined the proper-

ties of two-electron, two-minima quantum-dot molecules (QDM) in a magnetic field. The ground state as a function of magnetic field was found to have a highly non-trivial spin-phase diagram and a composite-particle structure of the wave function.<sup>12</sup> Also the calculated far-infrared absorption spectra in two-minima QDMs revealed clear deviations from the Kohn modes of a parabolic QD. Surprisingly, the interactions of the electrons smoothed the deviations instead of enhancing them.<sup>5</sup> In Ref. 47 we briefly discuss some of the results of square-symmetric four-minima QDM.

In this paper, we study in detail the properties of different QDMs. Three different QDM confinements are studied thoroughly and their properties are compared to parabolic-confinement single QDs. First, we calculate measurable quantities such as energy eigenstates, singlet-triplet splittings and magnetizations as a function of magnetic field. Secondly, non-measurable quantities, such as conditional densities, vortices, total densities, and the most probable positions are used to analyze the nature of the interacting electrons in quantum states and also to analyze and understand the properties of the measurable quantities. This paper is an extension to our previous calculations of QDMs.<sup>12,47</sup> We study a two-minima QDM (double dot), a square-symmetric four-minima QDM and a rectangular-symmetric four-minima QDM. The aim of this paper is to study how the confinement potential affects the properties of interacting electrons in a low-symmetry QD.

This paper is organized as follows: In Section II we explain how the quantum-dot molecules are modeled and what kind of basis we use in the exact diagonalization method. We also discuss calculation of magnetizations and the conditional single-particle wave function which we use to locate the vortices and study the conditional density. In the following four sections we present our results. In Section III we discuss properties of a single parabolic quantum dot, and in Sec. IV we analyze the properties of a double dot. In Sec. V we present results for the square-symmetric four-minima quantum-dot molecule, and finally in Sec. VI the results for rectangular four-minima quantum-dot molecule. The analysis of the results is presented in Section VII. The summary is given in Section VIII.

## II. MODEL AND METHOD

We model the two-electron QDM with the two-dimensional Hamiltonian

$$H = \sum_{i=1}^2 \left( \frac{(-i\hbar\nabla_i - \frac{e}{c}\mathbf{A})^2}{2m^*} + V_c(\mathbf{r}_i) \right) + \frac{e^2}{\epsilon r_{12}}, \quad (1)$$

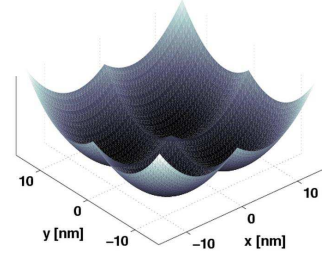


FIG. 1: Confinement potential of square-symmetric ( $L_x = L_y = 5$  nm) four-minima quantum dot molecule.

where  $V_c$  is the external confinement potential taken to be

$$V_c(\mathbf{r}) = \frac{1}{2}m^*\omega_0^2 \min \left[ \sum_j^M (\mathbf{r} - \mathbf{L}_j)^2 \right], \quad (2)$$

where the coordinates are in two dimensions  $\mathbf{r} = (x, y)$  and the  $\mathbf{L}_j$ 's ( $\mathbf{L}_j = (\pm L_x, \pm L_y)$ ) give the positions of the minima of the QDM potential, and  $M$  is the number of minima. When  $\mathbf{L}_1 = (0, 0)$  (and  $M = 1$ ) we have a single parabolic QD. With  $M = 2$  and  $\mathbf{L}_{1,2} = (\pm L_x, 0)$  we get a double-dot potential. We also study four-minima QDM ( $M = 4$ ) with minima at four possibilities of  $(\pm L_x, \pm L_y)$  (see Fig. 1). We study both square-symmetric ( $L_x = L_y$ ) and rectangular-symmetric ( $L_x \neq L_y$ ) four-minima QDMs. The confinement potential can also be written using the absolute values of  $x$  and  $y$  coordinates as

$$V_c(x, y) = \frac{1}{2}m^*\omega_0^2 \times [r^2 - 2L_x|x| - 2L_y|y| + L_x^2 + L_y^2]. \quad (3)$$

For non-zero  $L_x$  and  $L_y$ , the perturbation to the parabolic potential comes from the linear terms of  $L_x$  or  $L_y$  containing also the absolute value of the associated coordinate.

We use the GaAs material parameters  $m^*/m_e = 0.067$  and  $\epsilon = 12.4$ , and the confinement strength  $\hbar\omega_0 = 3.0$  meV. This confinement corresponds to the harmonic oscillator length of  $l_0 = \sqrt{\hbar/\omega_0 m^*} \approx 20$  nm. We concentrate on closely coupled QDMs where  $L_{x,y} \leq l_0$ . The magnetic field (in  $z$  direction) is included in the symmetric gauge by the vector potential  $\mathbf{A}$ . The Hamiltonian of Eq. (1) is spin-free, and the Zeeman energy can be included in the total energy afterwards ( $E_Z = g^* \mu_B B S_Z$  with  $g^* = -0.44$  for GaAs). We disregard the threefold splitting of each triplet state ( $S_Z = 0, \pm 1$ ) and consider only the lowest energy one ( $S_Z = 1$ ).

We drop the explicit spin-part of the wave function and expand the many-body wave function in symmetric functions for the spin-singlet state ( $S = 0$ ) and anti-

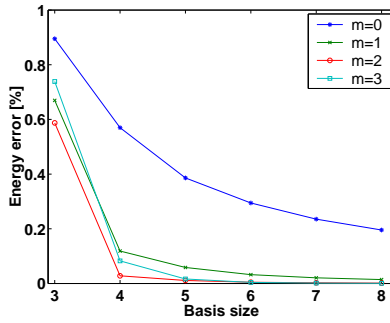


FIG. 2: Relative error in the energy of parabolic two-electron QD at  $B = 0$  as a function of the basis size  $n_x = n_y$  from 3 to 8, which corresponds to around 40–2000 many-body basis functions in the expansion. The relative angular momentum state of electrons is denoted with  $m$ .

symmetric functions for the spin-triplet state ( $S = 1$ ).

$$\Psi_S(\mathbf{r}_1, \mathbf{r}_2) = \sum_{i \leq j} \alpha_{i,j} \{ \phi_i(\mathbf{r}_1) \phi_j(\mathbf{r}_2) + (-1)^S \phi_i(\mathbf{r}_2) \phi_j(\mathbf{r}_1) \}, \quad (4)$$

where  $\alpha_{i,j}$ 's are complex coefficients. The one-body basis functions  $\phi_i(\mathbf{r})$  are 2D Gaussians.

$$\phi_{n_x, n_y}(\mathbf{r}) = x^{n_x} y^{n_y} e^{-r^2/2}, \quad (5)$$

where  $n_x$  and  $n_y$  are positive integers. The complex coefficient vector  $\alpha_l$  and the corresponding energy  $E_l$  are found from the generalized eigenvalue problem where the overlap and Hamiltonian matrix elements are calculated analytically. The matrix is diagonalized numerically.

The basis is suitable for closely coupled QDs. At large distances and at high magnetic field we expect less accurate results. The accuracy may also depend on the symmetry of the state. At zero magnetic field the *parabolic* two-electron QD can be modeled with a very good precision by expanding the basis (in a given symmetry) in relative coordinates. In Fig. 2 we compare the energy of the very accurate solution and the one using our basis (for a parabolic QD) as a function of the basis size, where the maximum  $n_x = n_y$  ranges from 3 to 8. These values correspond to around 40 – 2000 many-body configurations in the expansion. States with  $m = 0, 1, 2, 3$  refer to different relative angular momentum states. The relative error, even with the smallest basis studied  $n_x = n_y = 3$ , is less than one percent and decreases rapidly with the increasing basis size. The greatest error is found for the  $m = 0$  state.

The magnetization can be calculated as the derivative of the total energy with respect to magnetic field. It can be divided into to parts, paramagnetic and diamagnetic,

$$M = -\frac{\partial E}{\partial B} = \langle \Psi | \frac{e}{2m^*c} L_z + g^* \mu_B S_z | \Psi \rangle - \frac{e^2}{8m^*c^2} \langle \Psi | \sum_i r_i^2 | \Psi \rangle B, \quad (6)$$

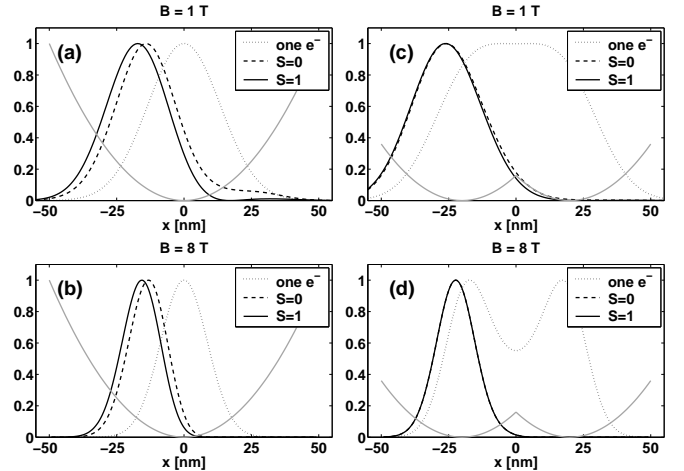


FIG. 3: One-body density (dotted line), two-body spin-singlet state (dashed line) and two-body spin-triplet state (solid line) along  $x$  axis. One of the electrons is fixed at the most probable position in the  $x$  axis ( $x^*$ ) and the conditional density is plotted for the other electron ( $|\psi_c(\mathbf{r})|^2 = |\Psi_S[(x, y), (x^*, 0)]|^2 / |\Psi_S[(-x^*, 0), (x^*, 0)]|^2$ ). The peaks on the left-hand side also indicates the most probable position, therefore by reflecting the peak position to the right-hand side of the  $x$  axis one can perceive the position of the fixed electron. (a) and (b) show the densities of parabolic QD at two different magnetic field values ( $B = 1$  and  $8$  T), (c) and (d) represent two-minima QDM with  $L_x = 20$  nm. The confinement potential,  $V_c$ , is plotted with gray color on each figure.

where the former is constant as a function of magnetic field, for a given angular momentum and spin state, and the latter depends linearly on magnetic field. The diamagnetic contribution to the magnetization is also a measure of the spatial extension of the ground state.<sup>38</sup>

Total electron density can be obtained by integrating one variable out from the two-body wave function

$$n(\mathbf{r}_1) = \int d\mathbf{r}_2 |\Psi_S(\mathbf{r}_1, \mathbf{r}_2)|^2. \quad (7)$$

In practice we do not perform numerical integration. The density is directly calculated in our diagonalization code where the required matrix elements are calculated analytically.

We analyze the two-body wave function by constructing a conditional single-particle wave function

$$\psi_c(\mathbf{r}) = |\psi_c(\mathbf{r})| e^{i\theta_c(\mathbf{r})} = \frac{\Psi_S[(x, y), (x_2^*, y_2^*)]}{\Psi_S[(x_1^*, y_1^*), (x_2^*, y_2^*)]}, \quad (8)$$

where one electron is fixed at position  $(x_2^*, y_2^*)$  and the density ( $|\psi_c(\mathbf{r})|^2$ ) and phase ( $\theta_c(\mathbf{r})$ ) of the other electron can be studied. One of the electrons is usually fixed at the most probable position  $(x_2^*, y_2^*)$ , but we also analyze  $\psi_c(\mathbf{r})$  when the other electron is fixed at some other position. The most probable positions of electrons  $(\mathbf{r}_1^*, \mathbf{r}_2^*)$  are found by maximizing the absolute value of the wave function with respect to coordinates  $\mathbf{r}_1$  and  $\mathbf{r}_2$ :

$$\max_{\mathbf{r}_1, \mathbf{r}_2} |\Psi_S(\mathbf{r}_1, \mathbf{r}_2)|^2 \rightarrow \mathbf{r}_1^*, \mathbf{r}_2^*. \quad (9)$$

One should note that  $|\psi_c(\mathbf{r})|^2$  is *not* normalized to one when integrated over the two-dimensional space because it describes the electron at position  $(x, y)$  on the condition that the other electron is fixed at  $(x_2^*, y_2^*)$ . Instead,  $|\psi_c(\mathbf{r})|^2$  is normalized so that it equals to one when  $x = x_1^*, y = y_1^*$ . Using the conditional single-particle wave function we can study the conditional density  $|\psi_c(\mathbf{r})|^2$  and the phase  $\theta_c(\mathbf{r})$ .

To illustrate how the properties of the many-body wave function can be examined with the conditional single-particle wave function, we compare interacting two-body conditional densities to non-interacting two-body densities in Fig. 3. The non-interacting two-body density is the same as the single-particle density (up to a normalization). We call it the one-body density hereafter. We plot the one-body, two-electron singlet ( $S = 0$ ) and two-electron triplet ( $S = 1$ ) conditional single-particle densities along  $x$ -axis. The other electron, in the two-electron systems, is fixed at the most probable position ( $x^*$ ) on the right-hand side of the  $x$ -axis.

Fig. 3 (a) and (b) show conditional densities of the single parabolic QD at  $B = 1$  and 8 T magnetic fields. The one-body density is located at the center since no correlation effects push it towards the edges of the dot. The peak of the triplet state is found further at the edge of the dot than the singlet peak since Pauli exclusion principle ensures that the electrons of the same spin are pushed further apart than the electrons with the opposite spins. Notice that the conditional density of the triplet state goes to zero where the other electron is fixed, just before  $x = 20$  nm, whereas in the singlet state there is a finite probability to find the electron around the point of the fixed electron.

Fig. 3 (c) and (d) show the same data for  $L_x = 20$  nm two-minima QDM. In high magnetic fields and at large dot-dot separations the difference between singlet and triplet densities reduces. In QDMs, with a sufficiently large distance between the dots and in high magnetic field also the one-body density localizes into the individual dots (see Fig. 3 (d)).

### III. PARABOLIC TWO-ELECTRON QUANTUM DOT ( $L = 0$ )

We start our analysis from the single parabolic quantum dot. The two-electron parabolic QD is studied extensively in the literature but presenting results here serves as a good starting point for understanding properties of quantum dot molecules.

#### A. Energy levels

Energy levels of the parabolic QD are plotted in Fig. 4 as a function of magnetic field. Fig. 4 (a) shows non-interacting two-body energy levels, (b) the ten lowest levels for two-body spin-singlet states ( $S = 0$ ), and (c)

for two-body spin-triplet ( $S = 1$ ) states. In (d) three lowest singlet and triplet levels are shown in the same plot. The non-interacting spectrum is obtained by occupying two electrons in the Fock-Darwin energy levels. The first eigenvalue at zero field equals two times ( $N_e = 2$ ) the confinement potential ( $\hbar\omega_0 = 3$  meV,  $E_1(B = 0) = 3 + 3 = 6$  meV) and the second level represents one electron in the lowest Fock-Darwin level and the other electron in the next one ( $E_2(B = 0) = 3 + 6 = 9$  meV). Many non-interacting energy levels are degenerate, also as a function of magnetic field. (In a less symmetric confinement, the degeneracies are lifted). Due to degeneracies, only six levels are seen in Fig. 4 (a). If the interactions are included, the spectra become much more complicated and many more level crossings are observed. One can also see how the energy scale is modified. In the spin-singlet spectra the ground state energy is almost doubled if the Coulomb interaction is included.

To see the crossing singlet and triplet states more clearly, we plot the three lowest energy levels of spin singlet (dashed line) and spin triplet (solid line) in Fig. 4 (d) up to  $B = 6$  T. In a weak magnetic field the ground state of the two-electron QD is spin-singlet ( $S = 0$ ), which changes to spin-triplet ( $S = 1$ ) as the magnetic field increases and then again to singlet and finally to triplet (at  $B \approx 6.3$  T, not visible in Fig. 4 (d)).

#### B. Singlet-triplet splitting and magnetization

In Fig. 5 (a) we plot the energy difference of the lowest triplet and singlet states up to  $B = 8$  T. Altering singlet and triplet states are also seen in higher magnetic fields with a decreasing energy difference between the states. However, if one includes the Zeeman term, the triplet state is favored over the singlet state at high  $B$ . Therefore the system becomes spin polarized.

The transitions between the states can also be examined from the magnetization curves plotted in Fig. 5 (b). The non-interacting magnetization is a smooth curve as no crossings are present in the lowest energy level. The orbital angular momentum in the non-interacting two-electron ground state does not change, and thus only the diamagnetic effects are seen in the magnetization. The non-interacting electrons have a smaller spatial extent of the wave function compared to the interacting electrons. Therefore, at low fields, when the response is purely diamagnetic, the magnetization curve of interacting electrons has a lower absolute value in Fig. 5 (b). The magnetization curve of interacting electrons shows abrupt increase of the otherwise smooth curve whenever two levels cross (see also Fig. 4 (d)). The peaks in magnetization are solely due to interactions.

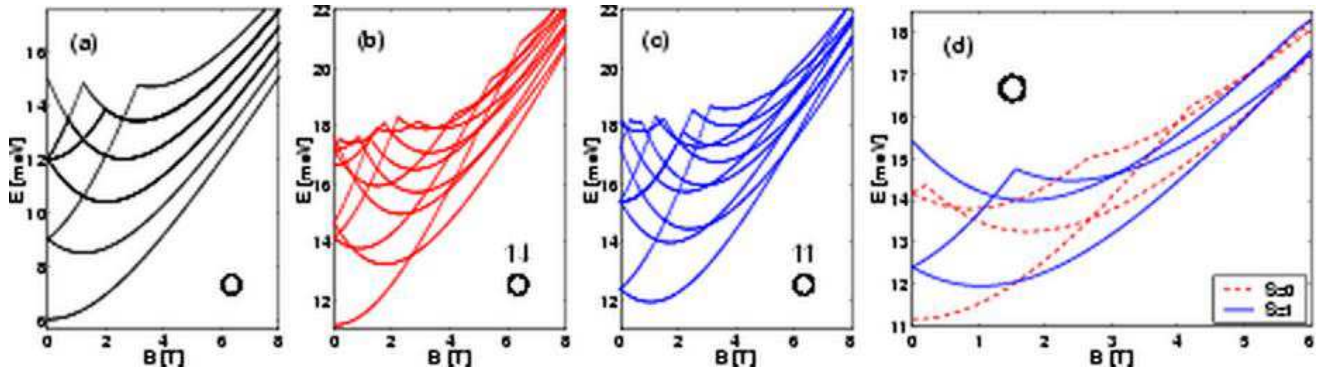


FIG. 4: Ten lowest energy levels of parabolic QD ( $L_x = 0, L_y = 0$ ) as a function of magnetic field of (a) non-interacting two-body, (b) two-body singlet state ( $S = 0$ ) and (c) two-body triplet state ( $S = 1$ ). Some of the states in (a) are degenerate. (d) three lowest energy levels of singlet (dashed line) and triplet (solid line) as a function of magnetic field up to  $B = 6$  T for parabolic QD ( $L_x = L_y = 0$ ). In (b) the first singlet ground state corresponds to angular momentum  $m = 0$  which changes to  $m = 2$  at  $B \approx 2.7$  T. In (c) the first triplet ground state is  $m = 1$  and it changes to  $m = 3$  at  $B \approx 5.8$  T. In (d) the first ground state equals to  $m = 0$  singlet, then ground state is  $m = 1$  triplet followed by  $m = 2$  singlet and  $m = 3$  triplet, where the latter is not visible as a ground state in (d). Zeeman energy is included in the triplet energies ( $E_Z = -2 \times 12.7B[T]$   $\mu$ eV in GaAs).

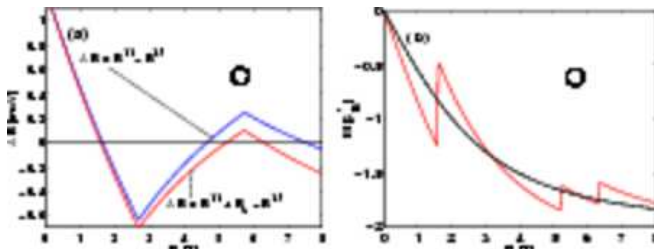


FIG. 5: Triplet-singlet energy difference in (a) and magnetization in (b) for parabolic QD ( $L_x = L_y = 0$ ). The lower curve in (a) shows the singlet-triplet splitting with Zeeman energy included. The smooth curve in (b) represents the magnetization of two non-interacting electrons and the other curve shows the magnetization for two interacting electrons. At low magnetic field values, the ground state is the angular momentum  $m = 0$  singlet, which shows as positive values in the triplet-singlet energy difference of (a) and as a smooth curve in (b). When the first transition from  $m = 0$  singlet to  $m = 1$  triplet occurs triplet-singlet energy difference changes its sign from positive to negative and there appears a peak in magnetization. Change of  $m = 1$  triplet to  $m = 2$  singlet and from  $m = 2$  singlet to  $m = 3$  triplet appear in the same way as peaks in magnetization and changes of sign in triplet-singlet splitting. Magnetization is given in the units of effective Bohr magnetons  $\mu_B^* = e\hbar/2m^*$  ( $\mu_B^* = 0.87$  meV/T for GaAs).

### C. Wave function analysis & vortices

We will now analyze the two-body wave functions and study in more detail singlet-triplet transitions in the single QD. The first singlet-triplet transition can be understood with the simple occupation of the lowest single-particle states: In the singlet state the two electrons occupy the lowest energy eigenstate with opposite spins ( $S = 0$ ). As the magnetic field increases, the energy difference between the lowest and the second low-

est single-particle levels decreases. (See non-interacting energy levels in Fig. 4 (a)). At some point the exchange energy in the spin-triplet state becomes larger than the energy difference between the adjacent energy levels. Thus, the singlet-triplet transition occurs and the adjacent eigenlevels are occupied with electrons of parallel spins ( $S = 1$ ).

However, the true solution of the two-electron QDM is much more complicated than the occupation of single-particle levels and inclusion of exchange energies. Interaction between the electrons changes the situation drastically. This can already be seen by comparing the single-particle energy levels of Fig. 4 (a) to singlet and triplet energy levels in (b) and (c). As a signature of complex many-body features, many singlet-triplet transitions are seen as a function of  $B$ . There are two trends competing in the ground state of a quantum dot when the magnetic field increases. The magnetic field squeezes the electron density towards the center of the dot and the Coulomb repulsion of electrons increases at the same time as the electron density is forced to a smaller volume. At some point it is favorable to change to a higher angular momentum ground state, which pushes electron density further apart and reduces the Coulomb energy. Therefore as a function of the magnetic field a series of different angular momentum states are seen.

The altering singlet and triplet states can also be understood in terms of composite particles of electrons and attached flux quanta.<sup>49</sup> The starting point for understanding the ground state changes and flux quanta is to consider the two-electron parabolic QD (as discussed in this Section), which has an exact solution for the wave function of the form

$$\Psi = (x_{12} + iy_{12})^m f(r_{12}) e^{-(r_1^2 + r_2^2)/2}, \quad (10)$$

where  $x_{12} = x_1 - x_2$ ,  $y_{12} = y_1 - y_2$  and  $r_{12} = |\mathbf{r}_1 - \mathbf{r}_2|$  are the relative coordinates of the two electrons,  $m$  is the rela-

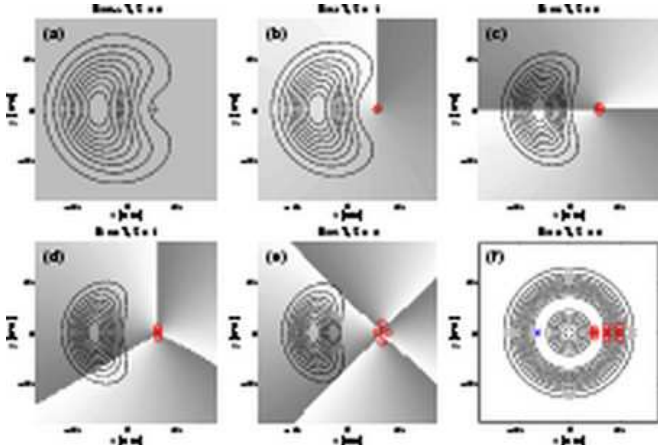


FIG. 6: (a)-(e) contours of *conditional* density  $|\psi_c(x, y)|^2$  and phase of the conditional wavefunction  $\theta_c(x, y)$  in gray-scale for parabolic QD ( $L_x = L_y = 0$ ). (White equals  $\theta_c = 0$  and darkest gray  $\theta_c = 2\pi$ ). Magnetic field value and the spin type are plotted on top of each figure. The plus sign (+) indicates the position of the fixed electron and small circles indicate the positions of the vortices. In (f) contours of *total* electron density of the three-vortex triplet state are plotted in the background and positions of the vortices are solved when the fixed electron is in three different positions. Fixed electron is marked with the plus sign and vortices with circles. The most probable position is marked with a star, on the left-hand side for clarity.

tive angular momentum and  $f$  is a correlation factor.<sup>12,50</sup> The zeros of the wave function (vortices in relative coordinates) are placed on  $z_{12} = x_{12} + iy_{12} = 0$  with a winding number given by the relative angular momentum  $m$ . In the first  $S = 0$  state the relative angular momentum of electrons is zero ( $m = 0$ ). When the magnetic field increases the ground state changes to spin triplet  $S = 1$ , where the relative angular momentum of electrons equals one ( $m = 1$ ) and in the second singlet state  $m = 2$ , and so on. With increasing magnetic field the relative angular momentum of electrons increases and altering singlet and triplet states are seen (if the Zeeman term is excluded). The transitions occur because in the states with large  $m$  the Coulomb repulsion becomes smaller at the cost of higher confinement and kinetic energies. As the increasing magnetic field squeezes electrons to a smaller area, it is favorable to move to larger  $m$  to minimize the total energy. One should note that with even  $m$  the spatial part of the total wave function is symmetric and therefore the spin part should be antisymmetric ( $S = 0$ ). With odd  $m$  the spin part is symmetric ( $S = 1$ ).

When the angular momentum increases, the increased rotation induces vortices in the system. As we have a many-body system, the rotation is a correlated motion of electrons and can be studied in the relative coordinates of electrons. Vortices can be found by locating the zeros of the wave function and studying the phase of the wave function when going around each of the zeros. As the vortices are seen in the relative coordinates, and are not

visible in the density, we examine the conditional single-particle wave function  $\psi_c(\mathbf{r})$  (of Eq. (8)), where one electron is fixed in the most probable position (on the  $x$  axis, the system is circular symmetric). The vortices are seen in the zeros of  $\psi_c$ . When the phase part,  $\theta_c$ , is integrated around a closed path encircling the zero, we obtain the winding number of the vortex ( $\oint \theta_c(\mathbf{r}) d\mathbf{r} = m2\pi$ ).

In a parabolic two-electron QD vortices are automatically attached on top of the electrons, where the relative angular momentum  $m$  equals the winding number of a vortex. In a less symmetric potential the center of mass and relative variables do not decouple and one would expect more complicated structures as can be seen in later sections. The simple form of the wave function in Eq. (10) is due to separation of the center of mass and relative coordinates in the parabolic confinement.

Calculated vortices and conditional densities of the single QD are shown in Fig. 6. The contours show the conditional electron density,  $|\psi_c|^2$ , and the gray-scale background marks the phase of the conditional wave function,  $\theta_c$ , where the white color equals  $\theta_c = 0$  and the darkest gray  $\theta_c = 2\pi$ . The positions of the vortices are marked with circles (o), and the other electron is fixed at the most probable position ( $\mathbf{r}_2^*$ ) shown with a plus sign (+). The lines of dark gray and white borders correspond to a sudden phase change of  $2\pi$  if the line is crossed. The number of flux quanta attached to the electron (or the winding number of a vortex) can be determined by going around the fixed electron position and calculating the total phase change (or counting the lines crossed in the figure).

In Fig. 6 (a) the phase is constant (no vortices and no relative angular momentum) and the the probability density of the other electron is located on the left side because of the Coulomb repulsion. In (b) we find one vortex as one border of white and gray is crossed when the fixed electron is encircled. In (c) we find two vortices, in (d) three vortices and in (e) four vortices. Fig. 6 (a) corresponds to the first singlet with relative angular momentum  $m = 0$ , (b) shows the first triplet with  $m = 1$ , (c) the second singlet with  $m = 2$  and (d) the second triplet with  $m = 3$ . Fig. 6 (e) would be the third singlet state but this is not a ground state if the Zeeman term is included. The conditional density shows how the electron localizes to a smaller area when the magnetic field increases. We also notice the enhancement of interaction at high  $B$  where the density contours are contracted compared to the low-field conditional densities.

The conditional density and phase are much more sensitive to the basis size than *e.g.* energy eigenvalues. In a parabolic QD the vortices should appear exactly on top of the fixed electron. However, in the two-, three- and four-vortex plots, in Fig. 6, the vortices are slightly displaced from the fixed electron position. The finite basis expansion does not result in exactly correct vortex picture. On the other hand, the problem is not very serious because the error in energy is not large and vortex positions are not experimentally observable and we also

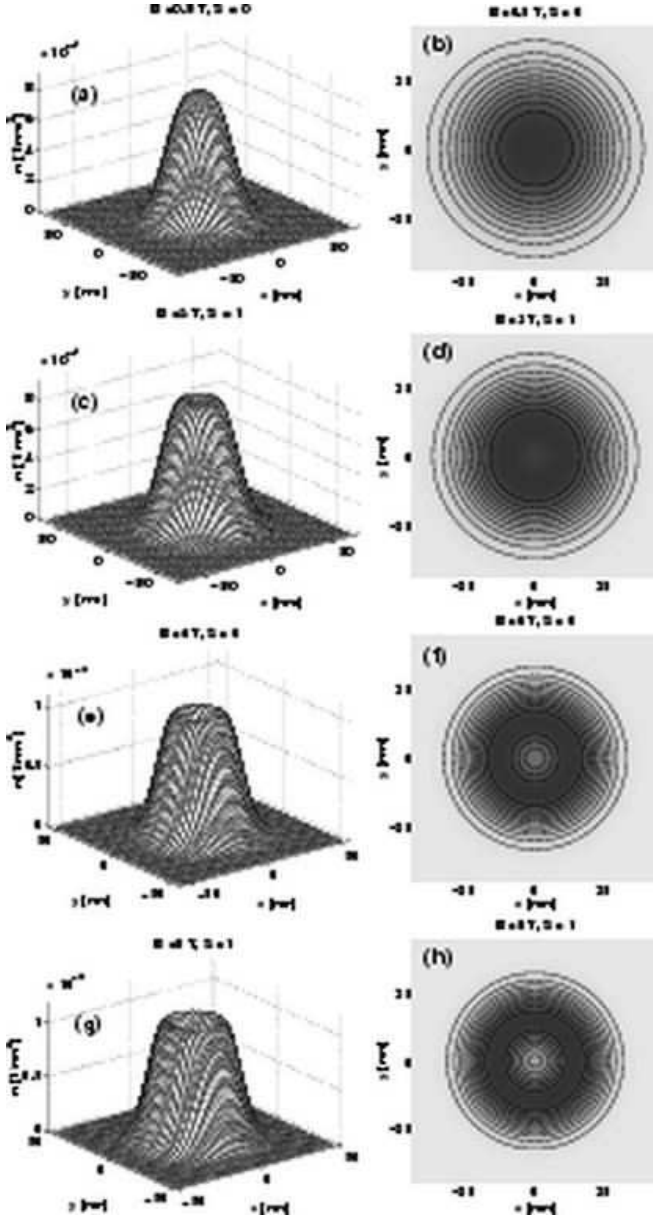


FIG. 7: Total electron density of the ground state at different magnetic field values for parabolic ( $L_x = L_y = 0$ ) QD. In the left column are densities in  $1/\text{nm}^2$  and on the right column are contours of the densities. Dark regions in the contours mark high density and brighter regions low density. Notice that in the densities the scale in the  $x$  and  $y$  axes is changing and the height of the peak is increasing with magnetic field. The range of axes in the contour plots is kept fixed. The magnetic field value and the spin type of the ground state is plotted above each sub-figure.

get correct winding numbers (angular momentum) if the pinned electron is encircled with a large enough radius.

Vortex dynamics can be studied if we change the position of the fixed electron. In Fig. 6 (f) we show the positions of the vortices in three different places of the fixed electron for the three-vortex triplet state. The to-

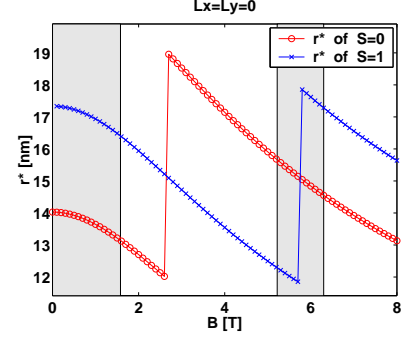


FIG. 8: Most probable position in nm of singlet ( $S = 0$ ) and triplet ( $S = 1$ ) states for parabolic ( $L_x = L_y = 0$  nm) QDM. The magnetic field region where singlet is a ground state is marked with gray background color.

tal electron density is shown in the background (see also Fig. 7 (g) and (h)). In a parabolic QD the vortices should be on top of the fixed electron no matter where it is pinned. Our calculations result wrongly a small offset of vortices from the fixed electron. Even if the vortices are not exactly on top of the fixed electron, and actually have a greater offset at greater distances from the origin, they are seen to follow the fixed electron if its position is changed. This is a signature of the composite particle nature of electrons and vortices.

#### D. Total electron density and the most probable position

In Fig. 7 we plot ground state total electron densities of the parabolic QD. The magnetic field values are the same as in Fig. 6 except that the four-vortex solution is not plotted since it is not a ground state. The range of both  $x$  and  $y$  axes and also the density in the  $z$  axis changes from (a) to (g) whereas in the contours the range of  $x$  and  $y$  is kept fixed. Dark regions in the contours mark high density and bright regions low density. As a function of magnetic field there forms a minimum in the center of the dot as the Coulomb repulsion forces electrons further apart. Note that even if there is a minimum in the total electron density, this is not a vortex. Vortices, in the composite particle picture, follow moving electrons and are seen in the relative coordinates of electrons. They describe the correlated motion of electrons and are not visible in an averaged-out quantity such as density.

Another way to study the nature of the changing ground states is to plot the most probable position (see Eq. (9)) as a function of magnetic field. Fig. 8 shows the most probable position ( $\mathbf{r}^*$ ) for both spin-singlet and spin-triplet states as a function of magnetic field. Gray background color indicates the region of magnetic field where the singlet is a ground state and white background color corresponds to magnetic field regions where the spin triplet is a ground state. Each jump in the curves corresponds to a change in the angular momentum. When the

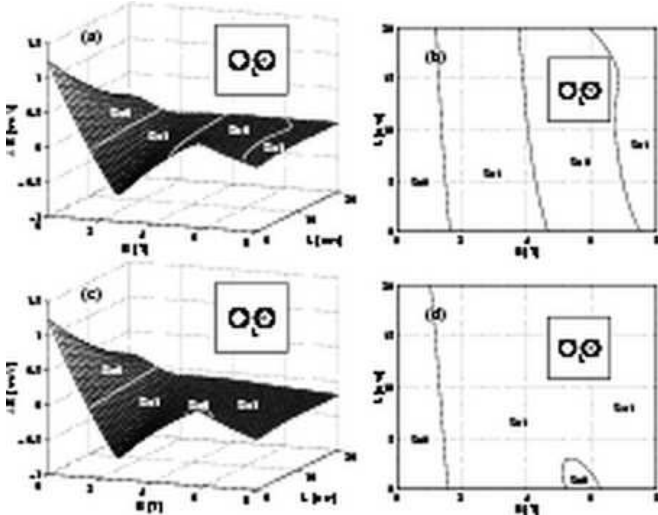


FIG. 9: Triplet-singlet energy difference ( $\Delta E = E^{\uparrow\uparrow} - E^{\uparrow\downarrow}$ ) as a function of magnetic field in two-minima quantum dot molecule. The energy difference is plotted as a function of dot-dot separation and magnetic field in (a) without Zeeman energy and in (c) with the Zeeman energy included ( $\Delta E = E^{\uparrow\uparrow} + E_Z - E^{\uparrow\downarrow}$ ). In (b) and (d) the ground state regions of the singlet and triplet states are plotted as function of  $B$  and  $L$ , without and with Zeeman energy, respectively.

singlet changes from  $m = 0$  to  $m = 2$  state at  $B \approx 2.7$  T the most probable position jumps to a higher value as well. See also energy level crossings in Fig. 4 (b). The outward relaxation, due to the increase of angular momentum, can be also seen in the density. Similar dependence is seen for the triplet state. First the most probable position decreases due to contracting electron density and then, at some point, it is favorable to move to a higher angular momentum state which relaxes the electron density outwards. In higher magnetic field we would see a sequence of transitions between increasing angular momentum states.

#### IV. TWO-MINIMA QUANTUM DOT MOLECULE ( $L_x \neq 0$ )

##### A. Singlet-triplet splitting as a function of $L$

In this section we study two laterally coupled quantum dots. In a two-minima QDM, or double dot, we study the changes in the ground state spectrum when two QDs, on top of each other, are pulled apart laterally. In Fig. 9 (a) the energy difference of the lowest triplet and singlet states is plotted as a function of the inter-dot spacing and magnetic field. At  $L = 0$  we have a single parabolic QD and the curve coincides with Fig 5 (a). When  $L \neq 0$  we have a double dot. Let us now examine some general trends of the triplet-singlet energy difference as a function of dot-dot separation. At small magnetic field the ground state is a spin singlet, then triplet, and again singlet as

in the single QD, but the transition points change and the energy differences are smaller at greater distances between the dots than in the single QD. The transition points and regions of singlet and triplet states are plotted in Fig 9 (b). We can also note that all transition points are shifted to lower  $B$  at large distances between the dots. If the Zeeman energy, that lowers the triplet energy, is included in the total energy the second singlet state disappears at greater  $L$  as can be seen in Fig. 9 (c) and (d). The second singlet is only seen in a small region with very closely coupled QDs ( $L \lesssim 2.5$  nm). Therefore, subsequent singlet states after the first one are not seen in the double dot if  $L \gtrsim 2.5$  nm. Similar results are seen in anisotropic QDs where the parabolic confinement of a single QD is elongated continuously to a wire-like confinement.<sup>27</sup>

##### B. Energy levels of $L_x = 5$ nm double dot

We choose one distance between the dots,  $L_x = 5$  nm, to study the properties of the double dot in more detail. We plot energy levels, singlet-triplet splitting, magnetization, vortices, the most probable position and total electron density of this double dot in Figs. 10 - 14. The energy levels in Fig. 10 are now modified, compared to the parabolic QD, due to the lower symmetry of the confinement potential. The circular symmetry is no longer present. The lower symmetry shifts and splits degenerate levels. The non-interacting levels, in Fig. 10 (a), split at zero magnetic field and there is also a small anticrossing of levels, just barely visible in the figure. Also degenerate levels of the single QD (see Fig. 4 (a)) are now slightly displaced in energy, which is mostly seen as thicker lines in Fig. 10 (a). In the interacting spectra, (b) and (c), we see many anticrossings. Also the nature of the lowest level does not change abruptly with crossing levels as in the single QD, but instead we see anticrossing levels. For example, there are clear anticrossings in the double dot singlet states of Fig. 10 (b) whereas states cross in the singlet state of parabolic QD of Fig. 4 (b).

We plot three lowest singlet and triplet energy levels in the same figure to see the transition points and energy differences between the states more clearly (Fig. 10 (d)). The ground state is a singlet at small  $B$ , also in the double dot, and later it changes to triplet. The Zeeman term lowers the triplet energy enough so that no second singlet (ground) state is observed at higher  $B$ , even though the singlet energy becomes very close to the triplet energy at  $B \approx 5$  T, as can be seen in Fig. 10 (d). The interesting anticrossing of spin singlet between  $B = 2$  and 3 T is now an excited state as the triplet is the ground state. We also find anticrossing ground state levels in the spin triplet around  $B \approx 5.5$  T, but the repulsion of levels is not so clear at high  $B$ .

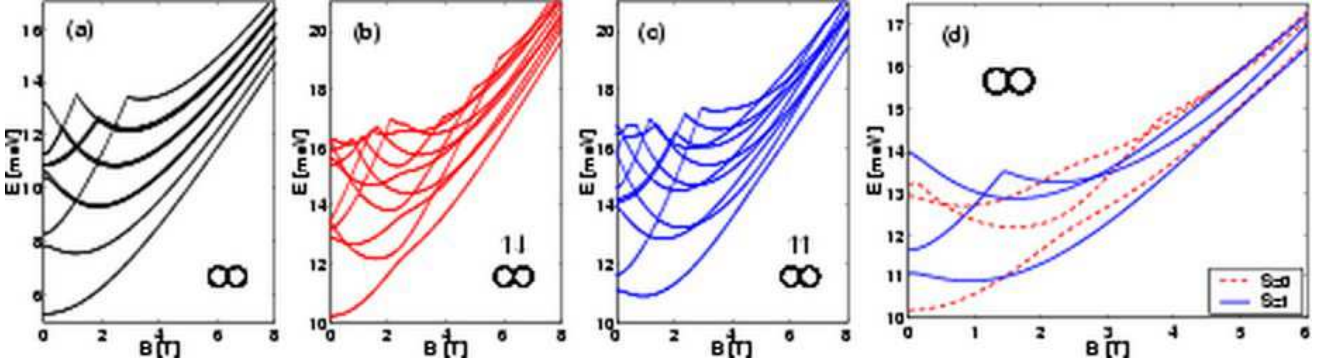


FIG. 10: Energy levels of  $L_x = 5, L_y = 0$  two-minima QDM. See Fig. 4 for details.

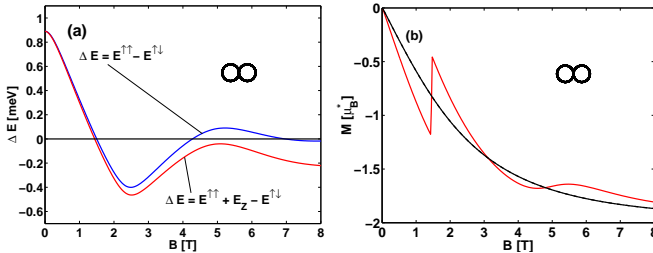


FIG. 11: Triplet-singlet energy difference (a) and magnetization (b) for  $L_x = 5, L_y = 0$  two-minima QDM. See Fig. 5 for details.

### C. Singlet-triplet splitting and magnetization of $L_x = 5$ nm double dot

The energy difference between the lowest triplet and singlet states as a function magnetic field in the  $L_x = 5$  nm double dot is plotted in Fig. 11 (a), and the magnetization in Fig. 11 (b). The sharp jump in the magnetization corresponds to the singlet-triplet transition. Even if the system is not circular symmetric, and angular momentum is not a good quantum number, there is an increase of the expectation value of angular momentum at the transition. We can clearly see that the magnetization increases suddenly at the transition point. Around  $B \approx 5.5$  T there is a bump in the magnetization. This is exactly at the anticrossing point of the triplet state. Therefore the symmetry of the triplet state changes or the magnetic moments of the electrons change. This time it is not seen as an abrupt change but as a continuous one. Similar magnetization curves are seen in asymmetric QDs with a correct deformation from the parabolic confinement to a more wire-like confinement.<sup>27</sup>

### D. Vortices of $L_x = 5$ nm double dot

In the case of QDMs the states cannot be identified with angular momentum since it is not a good quantum number. However, we can still study vortices and conditional density of the double dot. We fix one electron at

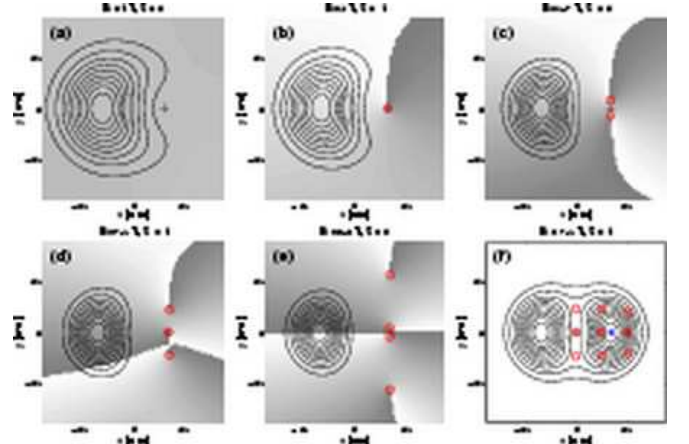


FIG. 12: (a)-(e) contours of conditional densities  $|\psi_c(x, y)|^2$  and phase of the conditional wavefunction  $\theta_c(x, y)$  in grayscale for  $L_x = 5, L_y = 0$  two-minima QDM. See Fig. 6 for details. (f) contours of total electron density of the three-vortex triplet state are plotted in the background and positions of the vortices with the fixed electron in three different positions.

the most probable position at  $\mathbf{r}^* = (x^*, 0)$  and study the conditional single-particle wave function

$$\psi_c(x, y) = \frac{\Psi_S[(x, y), (x^*, 0)]}{\Psi_S[(-x^*, 0), (x^*, 0)]}. \quad (11)$$

The most probable position of the two-minima QDM lies always on the  $x$  axis. In Fig. 12 (a), at low  $B$ , no vortices are found and the phase is constant. Contours are again localized to the left of the fixed electron having the maximum at  $(-x^*, 0)$ . The conditional density in a double dot is more localized compared to the conditional density of a single QD in Fig. 6 (a). The next plot, Fig. 12 (b) shows data for the triplet at  $B = 3.0$  T with one vortex and (c) shows the singlet state at  $B = 5.7$  T with two vortices, (d) the triplet at  $B = 7.5$  T with three vortices, and (e) the singlet at  $B = 8.2$  T with four vortices. The singlet state is not a ground state after the first singlet-triplet transition which means that two- and four-vortex solutions in (c) and (e) are only found as excited states.

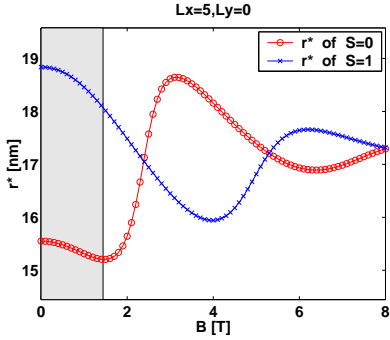


FIG. 13: Most probable position in nm of singlet ( $S = 0$ ) and triplet ( $S = 1$ ) states for two-minima ( $L_x = 5, L_y = 0$  nm) QDM. Singlet ground state magnetic field region is marked with gray background color.

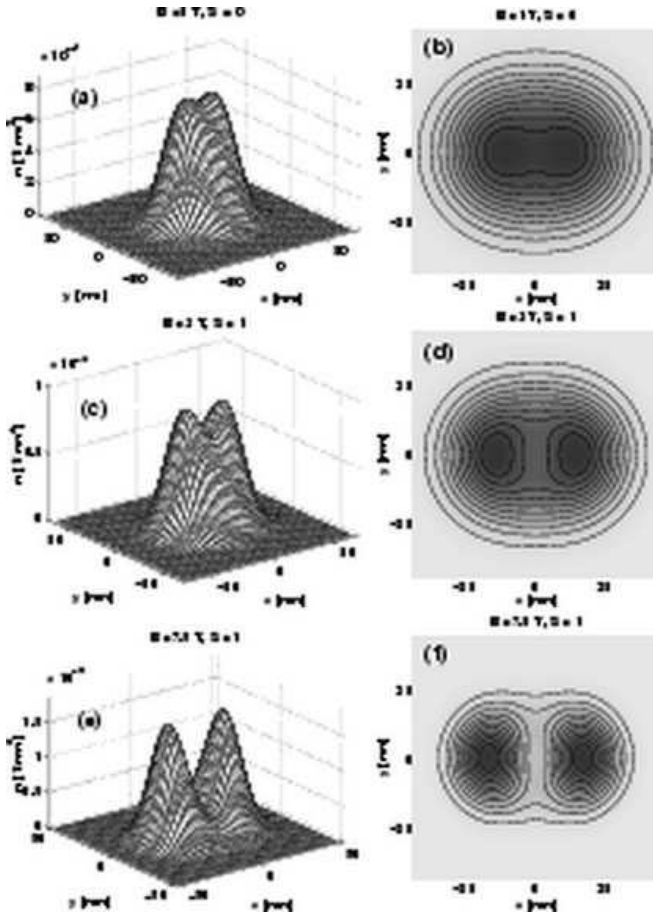


FIG. 14: Density of the ground state at different magnetic field values for two-minima ( $L_x = 5, L_y = 0$  nm) QDM. See Fig. 7 for details.

In the double dot vortices appear in the dot similarly as in the single QD. The vortices, on the other hand, are not exactly on top of the fixed electron, and they can be found at considerable distances from the fixed electron, as in Fig. 12 (e). Looking at the ground state at  $B = 7.5$  T in Fig. 12 (d) in more detail, it is interesting to see that

the vortices are seen in the vicinity of the fixed electron even if the conditional density is localized closer to the other dot and contour lines are rather circular though flattened in the  $x$  direction due to Coulomb repulsion. Despite the fact that the density of an electron is rather localized to one of the dots the two electrons move in a strongly correlated way in the double dot. The dynamics of vortices can be studied by changing the position of the fixed electron. In Fig. 12 (f) the electron is fixed in three different positions for the  $B = 7.5$  T triplet ground state. The *total* electron density is plotted in the background. The vortices follow the fixed electron which leads us to conclude that also in a non-symmetric potential flux quanta and electrons form composite particles. It is surprising to find composite particle solutions of electrons and flux quanta in the non-parabolic symmetry as well.<sup>12</sup>

The vortices are not exactly on top of the fixed electron. This may be in part due to the finite-size basis expansion, but on the other hand there is no reason why they should be *exactly* on top of the fixed electron. Interesting vortex clusters of a six-electron parabolic QD are studied in a recent article (Ref. 42) and also in elliptical and rectangular QDs in Ref. 45. In the double dot, the vortex patterns change continuously, where always an extra pair of vortices approach the fixed electron from minus and plus infinity from the  $y$  axis lying in the same vertical line with the fixed electron as in Figs. 12 (c)-(e).

#### E. Most probable position and total electron density of $L_x = 5$ nm double dot

The most probable position ( $\mathbf{r}^*$ ) for the lowest singlet and triplet states is plotted in Fig. 13. Due to the anti-crossing levels also the singlet and triplet most probable positions change continuously. A similar outward relaxation of the conditional density in the double dot is associated to the approaching vortices as was seen for the parabolic QD associated with the sudden change in the angular momentum state.

Ground state densities at three different magnetic field values are shown in Fig. 14. They show how the electron density localizes into the two minima as the magnetic field increases. The interacting density shows two peaks also in the low-field regime whereas the non-interacting density still has just one maximum (see the dotted line in Fig. 3 (c)).

#### V. SQUARE-SYMMETRIC FOUR-MINIMA QUANTUM-DOT MOLECULE ( $L_x = L_y \neq 0$ )

In this Section we study two electrons in lateral four-minima quantum-dot molecules. The minima are arranged in the way that they form a square in the lateral direction.

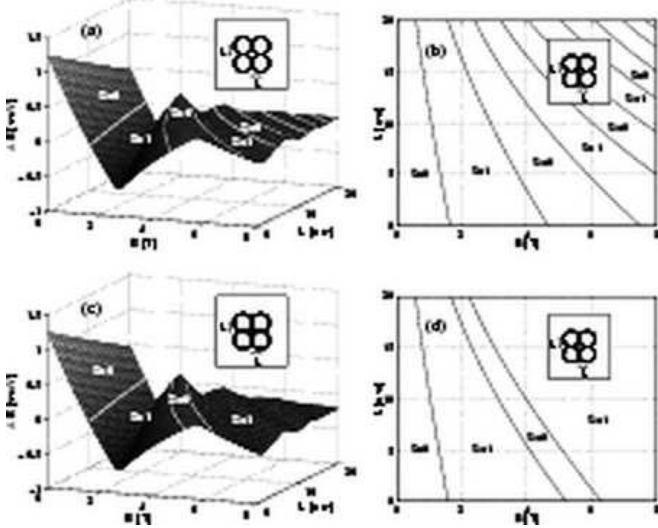


FIG. 15: Triplet-singlet energy difference ( $\Delta E = E^{\uparrow\uparrow} - E^{\uparrow\downarrow}$ ) as a function of magnetic field in square-symmetric ( $L = L_x = L_y$ ) four-minima quantum dot molecule. See Fig. 9 for details.

### A. Singlet-triplet splitting as a function of $L$

We study singlet and triplet states as a function of magnetic field and dot-dot separation. Fig. 15 (a) shows altering singlet and triplet states as a function of magnetic field. More frequent singlet-triplet changes are seen at greater separations between the dots (large  $L$ ). Also notable is the large energy difference of the second singlet state to the triplet state. The second singlet also persists as a ground state to the greatest studied separation  $L$ , which is not true in the double dot, if the Zeeman energy is included (Fig. 15 (c)). In all studied separations  $L$  the magnetic field evolution of the Zeeman coupled four-minima QDM (Figs. (c) and (d)) follows the same pattern. At small magnetic field values the ground state is singlet, then triplet and again singlet in a small magnetic field window before the ground state changes to triplet permanently. However, with large separations  $L$  the system becomes spin-polarized at lower magnetic field values, *i.e.* the border line of the second singlet and second triplet curves towards low-field region with increasing  $L$ .

We will now analyze the rapid changes of the singlet and triplet states of four-minima QDM. Singlet-triplet (and triplet-singlet) transition points shift to lower magnetic field values at greater  $L$ , where the area of the QDM ( $A$ ) is effectively larger. If the transitions occur at effectively the same values of the magnetic flux ( $\Phi = BA$ ), the transitions should be seen at lower  $B$  when the area is larger. This explains why the border lines between singlet and triplet states curve towards lower  $B$  at greater separations between the dots.

The second singlet is seen as a ground state in the Zeeman coupled system even at the very large distance of  $L = 20$  nm where the perturbation from a purely

parabolic potential is clear. However, in this type of square- or ring-like potential spatially symmetric states (singlet) are energetically more favorable than in elongated potentials (double dot) where in general the spatially antisymmetric states (triplet) are favored without paying too high price in Coulomb energy. Of course, as all energy scales are quite equal, the ground state is a delicate balance between kinetic, confinement and Coulomb energies as a function of magnetic field.

### B. Energy levels of $L_x = L_y = 5$ nm QDM

We will now focus on the  $L_x = L_y = 5$  nm four-minima QDM. The energy levels of non-interacting two-body, singlet and triplet states are plotted in Fig. 16 (a)-(c), respectively. In the square-symmetric four-minima QDM the *ground state* levels do not anticross as in the double dot, instead crossing ground states of the same spin state are seen, as in the single QD. However, the four-minima QDM is not circular symmetric and anticrossings are still seen in the higher energy levels, which is not the case with circular symmetric parabolic QD. Notice that in the non-interacting spectra in Fig. 16 (a) many levels are degenerate at  $B = 0$  for the four-minima QDM, whereas in the double dot the zero-field degeneracies are mostly lifted, see Fig. 10 (a). Yet, many levels that are degenerate in the single QD, Fig. 4 (a), as function of magnetic field, are slightly split in the non-interacting energy levels of four-minima QDM.

The singlet and triplet energies can be seen in the same plot in Fig. 16 (d). The energy levels of the four-minima QDM in Fig. 16 (d) look very similar to single QD energy levels of Fig. 4 (d). Even if the absolute values of energies and transition points are different, the only notable differences between parabolic QD and four-minima QDM are the small bending at zero field of the third triplet level, near  $E \approx 12.9$  meV, and small anticrossing of the uppermost triplet level at  $B \approx 1.3$  T.

### C. Singlet-triplet splitting and magnetization of $L_x = L_y = 5$ nm QDM

The energy difference between the lowest triplet and singlet and the magnetization are plotted in Fig. 17. Now, as no anticrossings of ground states are present, the triplet-singlet energy difference shows peaks. In the magnetization we also observe sharp peaks whenever two ground states cross. Similar results are seen in a square quantum dot with a repulsive impurity of Ref. 38 where the magnetization of two electrons in the dot shows sharp transitions since no anticrossings in the ground states are present. On the other hand, in a square QD with eight electrons slightly rounded magnetization curves are seen.<sup>26</sup> Therefore, if the circular symmetry of the confinement is broken, the magnetization depends on the symmetry of the confinement but also on the number of

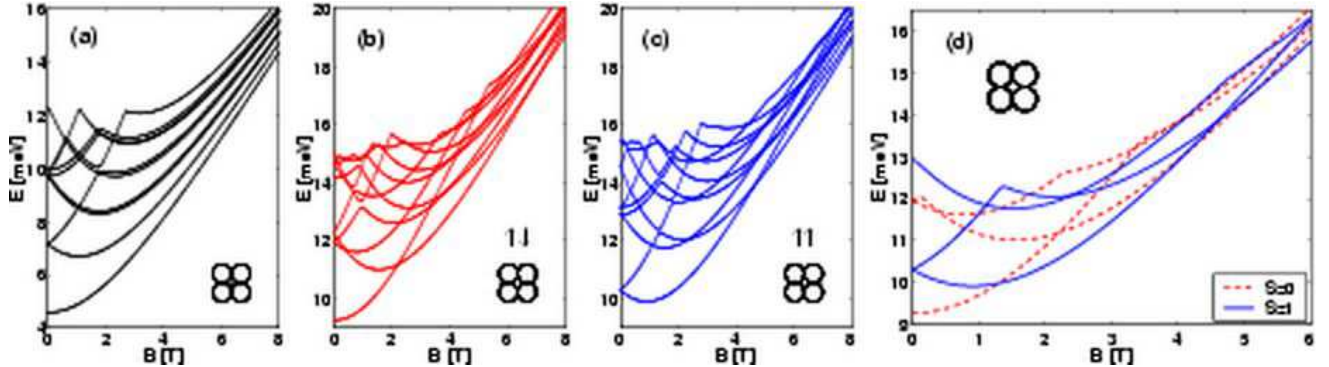


FIG. 16: Energy levels of  $L_x = L_y = 5$  nm four-minima QDM. See Fig. 4 for details.

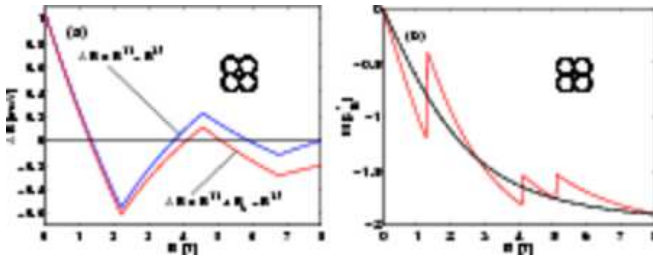


FIG. 17: Triplet-singlet energy difference in (a) and magnetization in (b) for  $L_x = L_y = 5$  nm QDM. See Fig. 5 for details.

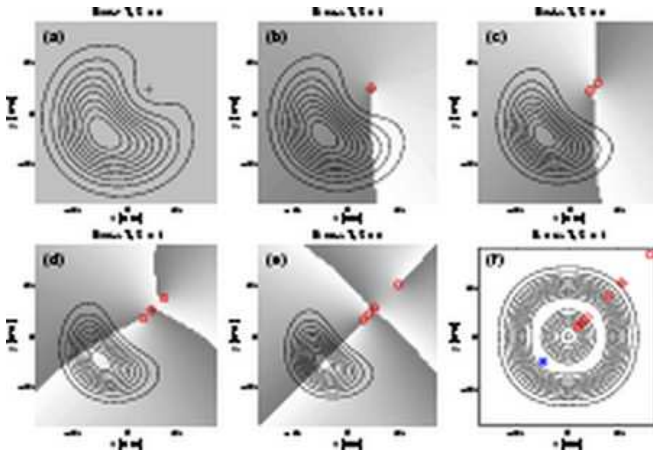


FIG. 18: (a)-(e) Contours of conditional densities  $|\psi_c(x, y)|^2$  and phase of the conditional wavefunction  $\theta_c(x, y)$  in grayscale for  $L_x = 5, L_y = 5$  four-minima QDM. See Fig. 6 for details. (f) contours of total electron density of the three-vortex triplet state are plotted in the background and positions of the vortices with the fixed electron in two different positions.

the electrons in the QD. It may not be straightforward to draw any conclusion about the underlying potential from the magnetization curves. Anticrossings, on the other hand, are clear signatures of a broken circular symmetry.

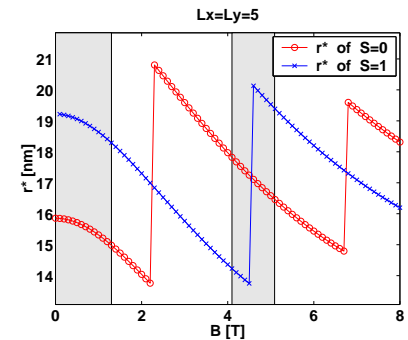


FIG. 19: Most probable position in nm of singlet ( $S = 0$ ) and triplet ( $S = 1$ ) states for four-minima  $L_x = L_y = 5$  nm QDM. Singlet ground state magnetic field region is marked with gray background color.

#### D. Vortices of $L_x = L_y = 5$ nm QDM

We can identify the changes in the magnetization to the increasing number of vortices in the two-electron QDM or to the increase of the expectation value of relative angular momentum of the electrons. Vortex patterns and conditional densities are shown in Fig. 18. The most probable position is now found from the line connecting two minima diagonally.

$$\psi_c(x, y) = \frac{\Psi_S[(x, y), (x^*, y^*)]}{\Psi_S[(-x^*, -y^*), (x^*, y^*)]}, \quad x^* = y^*. \quad (12)$$

At  $B = 0.7$  T in (a) the conditional density is spread to the area of three unoccupied dots with a peak in the furthest dot on the diagonal from the fixed electron. At high magnetic field the density becomes more localized closer to the most distant minimum, in the diagonal from the fixed electron. However, the contours show that the conditional density is not as circularly symmetric as in a double dot, but actually resembles more the conditional density of the single parabolic QD. The peak in the confinement potential at the origin seems not to affect the conditional density considerably when compared to the single QD. At high  $B$  the Coulomb repulsion forces elec-

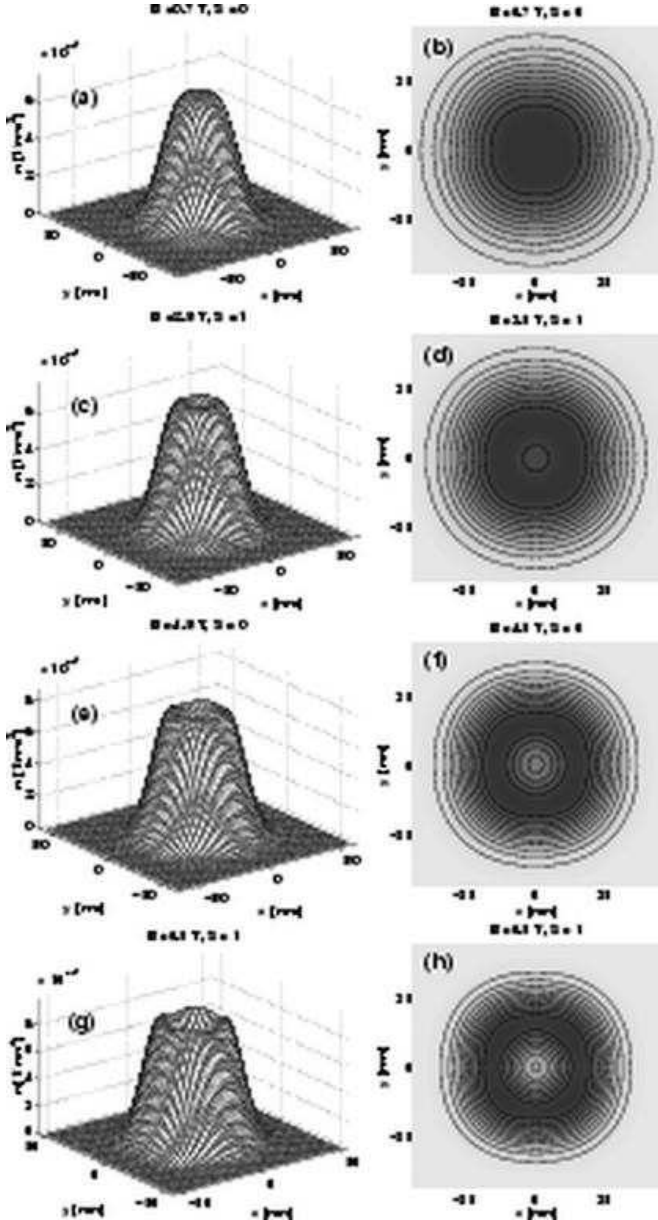


FIG. 20: Density of the ground state at different magnetic field values for four-minima  $L_x = L_y = 5$  nm QDM. See Fig. 7 for details.

tron density to the outer edges of the confinement, which might not result in very different results when compared to the single dot. However, the distance  $L_x = L_y = 5$  nm in the confinement is not particularly large and the perturbation from the parabolic confinement is not very large. On the other hand, altering singlet and triplet states persist to the greatest studied distance ( $L = 20$  nm) between the dots of  $L = 20$  nm where the perturbation from the parabolic confinement is clear.

The vortices appear in the four-dot QDM sequentially as a function of magnetic field. At low  $B$  the ground state is a singlet with no vortices, then a triplet with one vortex, a singlet with two vortices and then a triplet with

three vortices. The singlet with four vortices in Fig. 18 (e) is an excited state as the system becomes spin polarized after the two-vortex singlet state. The vortices are located in the diagonal going through the fixed electron position, see Figs. 18 (c)-(e). The vortices seem to be further away from the fixed electron (in the case of more than one vortex) than in the single QD. This is also true in the double dot. This could be identified to repulsion between the vortices but it is difficult to assess since the length scales are different due to different confinement strength and also the basis causes some errors. However, with six electrons in a parabolic confinement one can see a clear repulsion between the vortices.<sup>42</sup>

Vortex dynamics of the three-vortex solution is studied by changing the position of the fixed electron in Fig. 18 (f). Total electron density of the same state is plotted in the background of Fig. 18 (f). Vortices are seen to follow the fixed electron also in the four-minima QDM. However, in the four-minima QDM the vortices are further away from the fixed electron as the distance from the origin increases.

#### E. The most probable position and density of $L_x = L_y = 5$ nm QDM

The most probable positions of the lowest singlet and triplet states of the four-minima QDM (Fig. 19) show very similar behavior as the single QD. Only the most probable positions are on average roughly 2 nm greater at all field strengths compared to the single QD (size of the QDM is larger compared to single QD). Otherwise continuously decreasing  $\mathbf{r}^*$  shows a jump when the lowest singlet (or triplet) state changes.

Ground state densities and contours are plotted in Fig. 20. Starting from a rather flat density at low fields, a hole begins to form in the center as the magnetic field is increasing. The electron density localizes into a narrowing ring around the origin. However, compared to the parabolic QD, there are peaks forming in the four corners of the density, instead of a smooth density ring. Also the density looks more square-like in all of the contours.

#### VI. RECTANGULAR FOUR-MINIMA QUANTUM DOT MOLECULE ( $L_x \neq L_y \neq 0$ )

In this Section we examine the triplet-singlet energy difference, energy eigenlevels, magnetization, vortices, the most probable positions, and densities of four-minima QDM with rectangular positioning of the QD minima in the lateral plane.

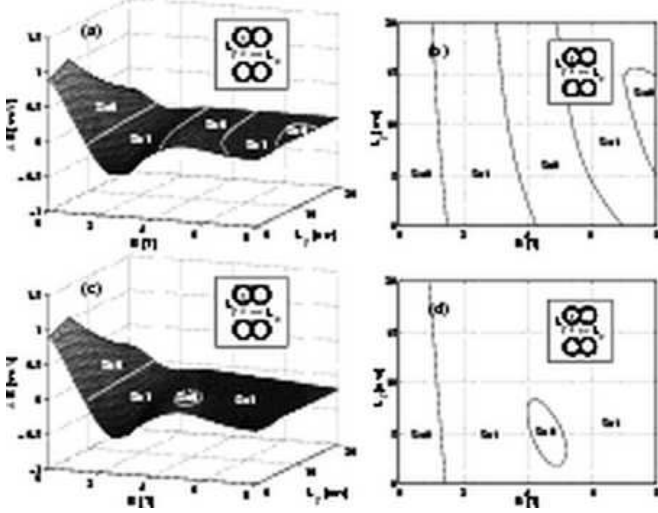


FIG. 21: Triplet-singlet energy difference ( $\Delta E = E^{\uparrow\uparrow} - E^{\uparrow\downarrow}$ ) as a function of magnetic field in rectangular-symmetric four-minima quantum dot molecule.  $L_x$  is fixed to 5 nm and  $L_y$  is varied from 0 to 20 nm. Therefore at  $L_y = 0$  we have  $L_x = 5$  nm double dot and at  $L_y = 5$  nm it is the square-symmetric four-minima QDM. The energy difference is plotted as a function of  $L_y$  and magnetic field in (a) without Zeeman energy and in (c) with the Zeeman energy included ( $\Delta E = E^{\uparrow\uparrow} + E_Z - E^{\uparrow\downarrow}$ ). In (b) and (d) the ground state regions of the singlet and triplet states are plotted as function of  $B$  and  $L_y$ , without and with Zeeman energy, respectively.

### A. Singlet triplet splitting as function of $L_y$ for fixed $L_x = 5$ nm rectangular QDM

The triplet-singlet energy difference of the rectangular QDM is plotted in Fig. 21. The distance between the minima in the  $x$  direction is fixed while the distance in the  $y$  direction is varied. We set  $L_x = 5$  nm and vary  $L_y$  from zero to 20 nm. Therefore, at  $L_y = 0$  we have a  $L_x = 5$  nm double dot, and at  $L_y = 5$  nm we have the  $L_x = L_y = 5$  nm square-symmetric four-minima QDM studied in the preceding section. The smooth surface in Fig. 21 is due to anticrossing ground states similarly as in the double dot. The anticrossings in the lowest levels of the singlet and triplet states are again present if the symmetry is distorted from a square to a rectangular symmetry, see the energy levels in Fig. 22. The only sharp peaks in Fig. 21 (a) and (c) correspond to rectangular symmetric QDM at  $L_x = L_y = 5$  nm.

One can also see that as a function of magnetic field singlet and triplet states do not change as rapidly as in the square-symmetric four-minima QDM. Interestingly, the third singlet region terminates around  $L_y \approx 15$  nm. So at sufficiently large distance between the two  $L_x = 5$  nm double dots the singlet state is no longer favorable even if the Zeeman term is excluded. In the case of a double dot in Ref. 12 it was not possible to say whether the second singlet state would terminate at greater distances between the dots, but for two double dots the third

singlet region clearly terminates.

If the Zeeman term is included (Figs. 21 (c) and (d)) the second singlet state can only be observed in a small region where the rectangular four-minima QDM is close to square symmetry (near  $L_y = 5$  nm). Actually the energy difference has its maximum, as function of  $L_y$ , at the square symmetry. If we follow the energy difference at zero magnetic field as a function of  $L_y$ , it first increases reaching the maximum at  $L_y = 5$  nm and then it decreases again when  $L_y$  is increased.

The stability of the singlet states (and also triplet states) in the *square*-symmetric QDM can be understood from the relatively high energy of the triplet state (or singlet) near the peak in  $\Delta E$ . In the square symmetry the degenerate energy levels at the crossing point are energetically very unfavorable. In rectangular symmetry degeneracies are lifted (anticrossings), which lowers the energy of the other spin type and also reduces the energy difference,  $\Delta E$ . Thus the energy differences are always smaller in the rectangular symmetry when anticrossings are present. The Jahn-Teller theorem states that any non-linear molecular system in a degenerate electronic state will be unstable and will undergo a distortion to form a system of lower symmetry and lower energy, thereby removing the degeneracy.<sup>48</sup> In a QDM, the system cannot, of course, lower the symmetry of the external confinement spontaneously to lift the degeneracies, but the large triplet-singlet energy differences in the square-symmetric QDM can be understood via Jahn-Teller effect: If the symmetry is lowered, degeneracies are lifted and smaller triplet-singlet energy differences are observed.

### B. Energy levels of $L_x = 5, L_y = 10$ nm QDM

We will now study rectangular  $L_x = 5, L_y = 10$  nm QDM in more detail. Fig. 22 (b) and (c) reveal many anticrossings in the interacting two-body spectra of  $L_x = 5, L_y = 10$  nm QDM, both in the ground states and also in the excited states. Many features look similar as in the double dot spectra in Fig. 10 but the anticrossing gaps are bigger here due to the greater separations between the dots (greater deviation from the circular symmetry). Fig. 22 (d) shows singlet and triplet energy levels in the same plot. The second singlet becomes very close to the triplet near  $B = 5$  T, but the triplet remains the ground state.

### C. Singlet-triplet splitting and magnetization of $L_x = 5, L_y = 10$ nm QDM

The energy difference of triplet and singlet states is plotted in Fig. 23 (a). The magnetization in Fig. 23 (b) show first a sharp peak which corresponds to singlet triplet transition. The next change is from the one-vortex triplet to the three-vortex triplet and as these two states

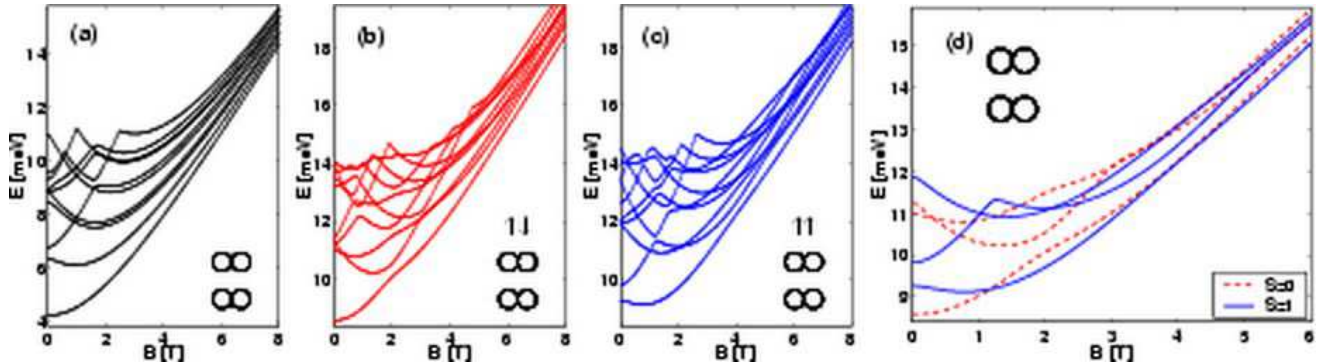


FIG. 22: Energy levels of  $L_x = 5, L_y = 10$  nm rectangular four-minima QDM. See Fig. 4 for details.

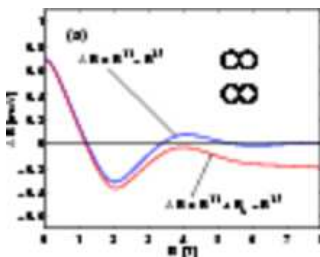


FIG. 23: Triplet-singlet energy difference (a) and magnetization (b) in  $L_x = 5, L_y = 10$  nm rectangular four-minima QDM. Magnetization is given in the units of effective Bohr magnetons  $\mu_B^* = eh/2m^*$ .

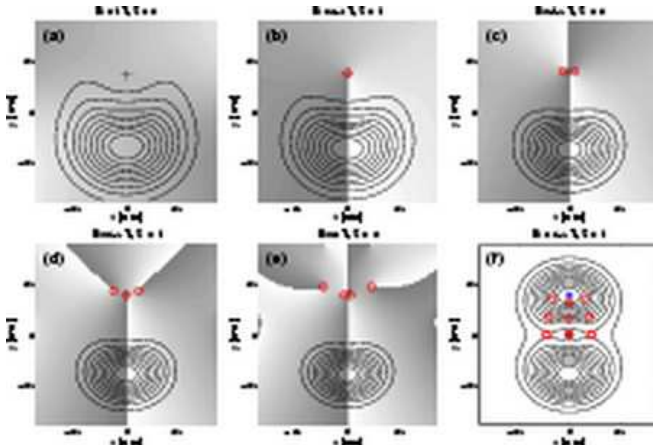


FIG. 24: (a)-(e) contours of conditional densities  $|\psi_c(x, y)|^2$  and phase of the conditional wavefunction  $\theta_c(x, y)$  in grayscale for  $L_x = 5, L_y = 10$  four-minima QDM. See Fig. 6 for details. (f) contours of *total* electron density of the three-vortex triplet state are plotted in the background and positions of the vortices with the fixed electron in three different positions.

anti-cross we see continuous increase of the magnetization before it starts to decrease again due to the contraction of the electron density. It is interesting that after the bump the interacting magnetization has very similar dependence on the magnetic field as the non-interacting

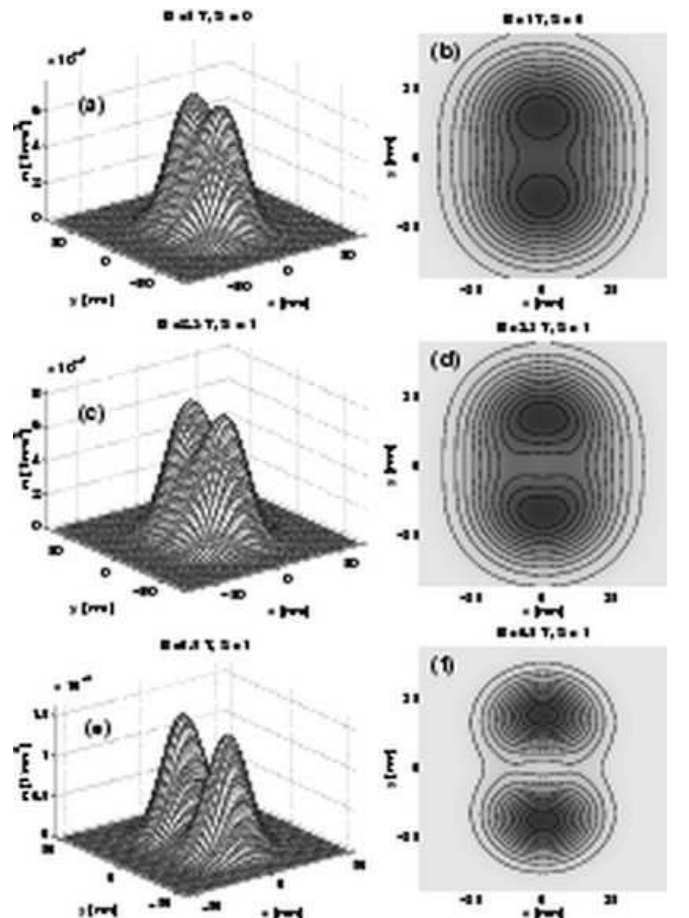


FIG. 25: Density of the ground state at different magnetic field values for  $L_x = 5, L_y = 10$  nm rectangular four-minima QDM. See Fig. 7 for details.

magnetization. At high enough magnetic field the electrons are localized into individual double dots and have single-particle properties and the spatial extents in the interacting and non-interacting systems are not very different (see Eq. (6)). However, the electrons may move in a correlated way even if they are localized into one of the double dots. One should remember that there is also

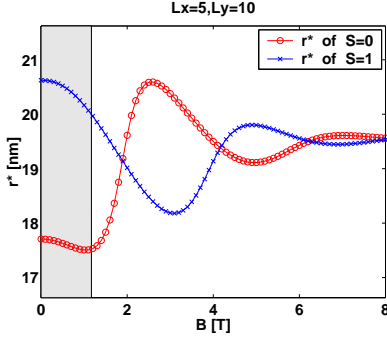


FIG. 26: Most probable position in nm of singlet ( $S = 0$ ) and triplet ( $S = 1$ ) states for rectangular-symmetric four-minima ( $L_x = 5, L_y = 10$  nm) QDM. Singlet ground state (magnetic field) region is marked with gray background color.

the paramagnetic part in the magnetization, but this is constant for a given state, if the the angular momentum is a good quantum number, and does not depend on the magnetic field. Of course, in a non-circular symmetry the paramagnetic magnetization may not be constant as a function of magnetic field.

#### D. Vortices of $L_x = 5, L_y = 10$ nm QDM

The phase information and the conditional densities of the rectangular four-minima QDM are shown in Fig. 24. The most probable position lies now on the  $y$  axis. Another possibility would be to have the most probable position on a line connecting the two minima diagonally. However, as the other double dot is left with just one electron and the distance of  $L_x = 5$  nm is so small that the single-particle density is not localized to the minima of the double dot. So the most probable position is in the  $y$  axis. In rectangular symmetry correlations force the one electron to one of the double dots. With small  $L_x$ 's conditional density shows a peak at  $x = 0$  as in the non-interacting two-body density in Fig. 3.

The conditional density becomes more localized as the magnetic field increases. The vortices appear sequentially in the QDM. The second and third singlet states (in Fig. 24 (c) and (e)) are not ground states as the system becomes spin-polarized after the first singlet-triplet transition. There is again a repulsion between the vortices. Interesting is to note that in (e) the two more distant vortices are positioned much closer to the fixed electron when compared to the double dot of Fig. 12 (e). The white and dark regions near the borders of Fig. 24 (e) show the shades of phase boundaries of more distant vortices (not visible in the figure).

Vortex dynamics is studied in Fig. 24 (f) for the three vortex triplet (at  $B = 6.5$  T). The electron is fixed at three different positions and the *total* electron density of the same state is plotted in the background. One vortex, or Pauli vortex, is always on top of the fixed electron

and the two additional vortices are symmetrically on the sides of the fixed electron. As the fixed electron is moved from the origin to the direction of the positive  $y$  axis, the vortices aside become closer to the fixed electron.

#### E. Total electron density and the most probable positions of $L_x = 5, L_y = 10$ nm QDM

Ground state electron densities in Fig. 25 show a localization into two double dots as the magnetic field is increased. If the densities would be rotated by 90 degrees they would resemble very much two-minima QDM (double dot) densities of Fig. 14. The smaller displacement ( $L_x = 5$  nm) in the four-minima QDM potential has a much smaller effect than the larger displacement ( $L_y = 10$  nm) because electrons localize into the double dots (with  $L_x = 5$  nm) separated from each other with a distance  $d = 2L_y = 20$  nm. Therefore electron density of rectangular four-minima QDM effectively resembles of that of a two-minima QDM (double dot). This is true for interacting two-electron system.

The most probable positions of the lowest singlet and triplet states are shown in Fig. 26. Continuously changing  $\mathbf{r}^*$  (*i.e.* no jumps) is due to anticrossing states where symmetry of a state (and also  $\mathbf{r}^*$ ) changes continuously. Interesting is the strong suppression of the oscillations of  $\mathbf{r}^*$  at greater  $B$ . At large magnetic field the electrons localize into a distant double dots and interaction effects (like changing angular momentum states in parabolic QD) have a smaller impact on the properties of the two-electron system. The effect is quite different for parabolic QD and square-symmetric four-minima QDM where the localization of electron density is not so strong due to the nature of the confinement potential.

## VII. ANALYSIS OF THE RESULTS AND THEIR RELEVANCE TO EXPERIMENTS

### A. Role of symmetry in quantum dot confinement

We start our analysis of the data presented above from the measurable quantities. One such observable is the total energy for ground and excited states as a function of the magnetic field, as well as the magnetization. To ease the comparison, these are collected in Fig. 27. The most striking feature is that the data of the the square-symmetric four-minima QDM is very similar to the one of the single parabolic dot. On the other hand, the data of the double dot resemble the one of a rectangular four-minima QDM. The reason behind the similarities of these pairs is the symmetry. The square-symmetric and circularly symmetric cases have higher symmetries than the rectangular ones. One can study this in detail by splitting the total Hamiltonian of Eq. (1) to two parts as  $H = H_0 + H_I$ , where  $H_0$  is the Hamiltonian of the parabolic case ( $L_x = L_y = 0$ ), and the impurity Hamilto-

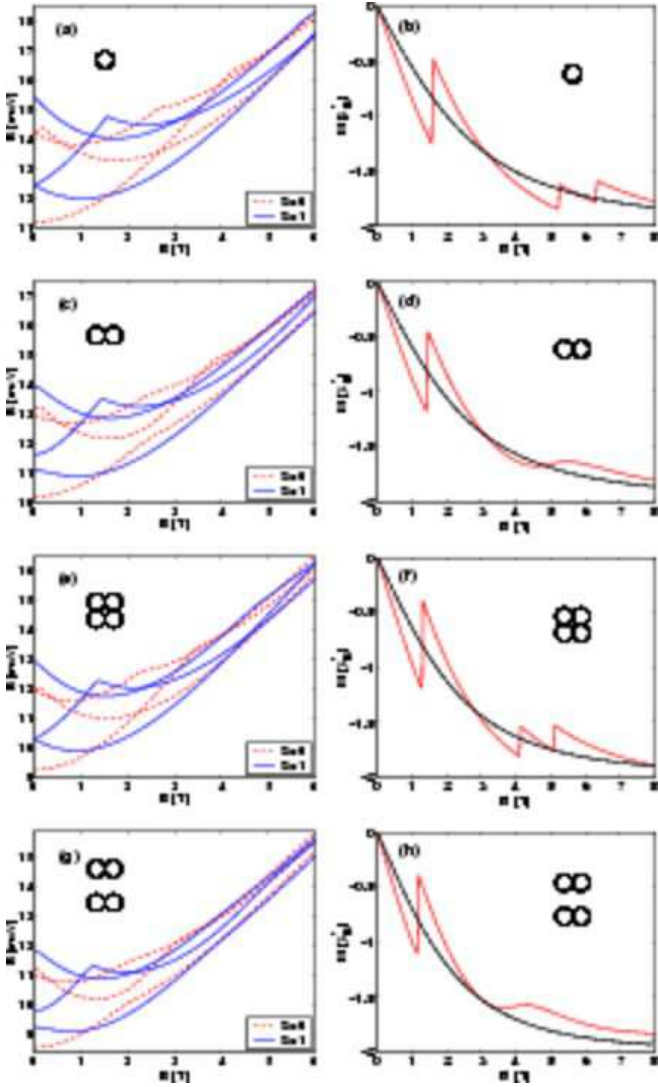


FIG. 27: Three lowest singlet and triplet energy levels and magnetization for all studied quantum dot confinements.

nian  $H_I$  contains the terms from finite  $L_x$  and  $L_y$  values, see Eq. (3). If we now have a high symmetry in the system, meaning  $L_x = L_y$ , one can see that the  $H_I$  does not couple the eigenstates of  $H_0$  that have a different symmetry. On the other hand, in the case with  $L_x \neq L_y$ ,  $H_I$  has a lower symmetry and more of the symmetries of  $H_0$  are broken. Due to this, states with different symmetry are coupled. This leads to anticrossings in the energies as seen in Fig. 27, where also the crossings of the high-symmetry cases are seen. One can estimate the strength of the symmetry-lowering part from the anti-crossing gap in energy, as in the point where the energies would cross, one has in the first approximation a Hamiltonian matrix:

$$H = \begin{pmatrix} E_0 & E_\delta \\ E_\delta & E_0 \end{pmatrix}, \quad (13)$$

where  $E_0$  is the energy at middle of the gap, and  $2E_\delta$  is the width of the gap.

The magnetization curve for the low- and high-symmetry cases are also very different, see Fig. 27. A common feature in all these cases is the sharp increase in magnetization at the point where the total spin of the ground-state changes. On the other hand, the low-symmetry anticrossings of the energy result smooth changes in magnetization, whereas the high-symmetry data show sudden jumps.

These findings indicate that it is rather difficult to obtain detailed information of the system based on the energetics and the magnetization. The symmetry of the system can be extracted, but not much beyond that. For larger particle numbers, more and more of the correlation effects can be captured by the mean-field level. The effective potential has, due to the Hartree potential, a higher symmetry than the mere external potential.<sup>5</sup> This results in less details to both energetics and the magnetization.

A similar role of the symmetry can be seen on the non-measurable quantities, like the densities. On the other hand, the vortices are more delicate. This is because they depend linearly on the wave function, unlike densities and energies that are second order.

## B. Exchange of two spins

The idea of double dot spin-swap operations in quantum computing<sup>14</sup> lies in the coherent rotation of two initially isolated spins. Starting with, say, spin-up electron in the left and spin-down electron in the right dot:  $|\uparrow\rangle_L|\downarrow\rangle_R$  and rotating spins to opposite order:  $|\downarrow\rangle_L|\uparrow\rangle_R$ . These would be initial and final states of the system. Coherent rotation between initial and final states requires entangled spin states like spin-singlet  $|S\rangle = (|\uparrow\rangle_L|\downarrow\rangle_R - |\downarrow\rangle_L|\uparrow\rangle_R)/\sqrt{2}$  and triplet  $|T_0\rangle = (|\uparrow\rangle_L|\downarrow\rangle_R + |\downarrow\rangle_L|\uparrow\rangle_R)/\sqrt{2}$  whereas the other two triplet states  $|T_+\rangle = |\uparrow\rangle_L|\uparrow\rangle_R$  and  $|T_-\rangle = |\downarrow\rangle_L|\downarrow\rangle_R$  are not conceivable as they have identical spins. The states described above are only for the spin-part of the wave function but of course the spatial part, discussed extensively in this paper for singlet and triplet eigenstates, must be modified along with the rotation.

In the simplified Heisenberg picture, rotation depends only on the singlet-triplet splitting energy,  $J = \Delta E = E^{\uparrow\uparrow} - E^{\uparrow\downarrow}$ , or exchange coupling of two spins.<sup>14</sup> Hubbard-type models can be used to study time evolution of a little bit more elaborate states.<sup>15,16</sup> To fully investigate the coherent rotation of two-electron system, it would be better to start with initially separated electrons (that can be constructed from many-body wave functions) and study the time evolution of the state in the exact many-body basis instead of using some simplified models. However, tuning  $J$  with dot-dot separation at small magnetic fields, the spin rotations can be quite safely modelled within the Heisenberg picture. At high magnetic fields, on the other hand, electrons in lateral double dots form finite quan-

tum Hall-like composite-particle states of electrons and flux quanta, as shown in this study and in previous studies.<sup>12,17</sup> Therefore, the coherent spin rotations at high  $B$  may be quite different from zero  $B$  rotations, even if  $J$  could have exactly same value for high- $B$  and zero- $B$  states. These states are of course of great scientific interest as their own, but from the perspective of coherent two-spin rotations they may function quite differently as suggested by the Heisenberg or Hubbard models. Electric control of  $J$  with dot-dot separation may also be advantageous in other perspectives because magnetic fields are more difficult to apply locally.

### C. Comparisons to experiments

In very recent experiments Petta *et al.* demonstrate a coherent rotation of two spins between singlet  $|S\rangle$  and triplet  $|T_0\rangle$  states in a lateral double dot device.<sup>25</sup> They start the operation from singlet state in single QD and then isolate two opposite spins in separated dots where the singlet-triplet splitting vanishes and no tunneling is allowed between the two dots. Coherent rotation is performed by bringing the two dots closer allowing small but finite energy splitting  $J$  between  $|S\rangle$  and  $|T_0\rangle$  states. Probability of finding singlet is measured as a function of gate operation time. Fig. 9 (a) of this study shows calculated singlet-triplet splitting as a function of dot-dot separation and magnetic field. Following the zero magnetic field line one and see how the singlet-triplet splitting decreases as a function of increasing dot-dot separation. Fixing  $B = 0.1$  T, as in the experiment, for single dot ( $L = 0$ ) we have  $J = 1.16$  meV and for double dot at the greatest interdot distance studied ( $d = 2L = 40$  nm) we have  $J = 0.16$  meV. Petta *et al.*<sup>25</sup> find three times smaller value in single QD ( $J = 0.4$  meV) as our calculations. This is simply a consequence of different quantum dot confinement energy  $\hbar\omega_0$ .

Lee *et al.* studied experimentally singlet-triplet splitting as a function of magnetic field in silicon two-electron double dot.<sup>18</sup> The measurements show very similar data as our results. The first singlet-triplet transition is resolved clearly in the experiment in accordance to our calculations. Decreasing the coupling between the dots results in a small shift of  $J = 0$  to low fields as in our results represented in Fig. 9. The high-field regime, where we would expect to find small  $J$  and even possibly a positive  $J$ , which would correspond second singlet ground

state, is not measured to very high field strengths. However, to fully compare our results to the measurements on silicon double dots we should recalculate our data with silicon effective mass and dielectric constant.

Brodskey *et al.*<sup>13</sup> were the first to measure ground state energy levels of a lateral two-electron double dot as a function of magnetic field. Even if they did not concentrate on two-electron case particularly, the line for two electrons is clearly visible in their data showing also a kink indicating the singlet-triplet transition.

Magnetization is very difficult to measure directly for just two electrons. However, indirect methods and direct methods with large arrays of individual few-electron dots may provide interesting experimental results.<sup>34,35</sup> Even if it is difficult to compare existing measurements of many electron dots to our two-electron system, the double dot measurements of Oosterkamp *et al.*<sup>34</sup> show similar type of anticrossings as our calculated magnetization curves.

## VIII. SUMMARY

In summary, we have thoroughly studied different lateral two-electron quantum-dot molecules. All our exact diagonalization calculations were performed for closely coupled quantum dots. Many-body electron wave functions were allowed to extend over the whole system. We have analyzed how the physical properties change when a deviation or disorder is introduced in the confinement potential of the symmetric quantum dot. We have calculated measurable quantities such as energy levels, singlet-triplet splitting, and magnetization as a function of magnetic field strength. The measurable quantities were further analyzed by calculating non-measurable quantities such as phase vortices and conditional densities. We have also compared the properties of non-interacting electrons to interacting ones in quantum dot molecules to separate the effects of the non-circular confinement potential and interactions.

## Acknowledgments

This work has been supported by the Academy of Finland through its Centers of Excellence Program (2000-2005).

\* Corresponding author: M. Helle before M. Marlo; Electronic address: Meri.Helle@hut.fi

<sup>1</sup> T. Chakraborty and P. Pietiläinen, *The Quantum Hall Effects: Fractional and Integral*, (Springer, Berlin, 1995).

<sup>2</sup> L. Jacak, P. Hawrylak, and A. Wójs, *Quantum Dots* (Springer, Berlin, 1998).

<sup>3</sup> P. A. Maksym and Tapash Chakraborty, Phys. Rev. Lett.

**65**, 108 (1990).

<sup>4</sup> M. Hochgräfe, Ch. Heyn, and D. Heitmann, Phys. Rev. B **63**, 035303 (2001).

<sup>5</sup> M. Marlo, A. Harju, and R. M. Nieminen, Phys. Rev. Lett. **91**, 187401 (2003).

<sup>6</sup> T. Chakraborty, V. Halonen, and P. Pietiläinen, Phys. Rev. B **43**, R14289 (1991).

<sup>7</sup> D. Pfannkuche and R. R. Gerhardts, Phys. Rev. B **44**, R13132 (1991).

<sup>8</sup> A. V. Madhav and T. Chakraborty, Phys. Rev. B **49**, 8163 (1994).

<sup>9</sup> I. Magnúsdóttir and V. Gudmundsson, Phys. Rev. B **60**, 16591 (1999).

<sup>10</sup> C. A. Ullrich and G. Vignale, Phys. Rev. B **61**, 2729 (2000).

<sup>11</sup> Tapash Chakraborty and Pekka Pietiläinen, Phys. Rev. Lett. **95**, 136603 (2005).

<sup>12</sup> A. Harju, S. Siljamäki, and R. M. Nieminen, Phys. Rev. Lett. **88**, 226804 (2002).

<sup>13</sup> M. Brodsky, N. B. Zhitenev, R. C. Ashoori, L. N. Pfeiffer, and K. W. West, Phys. Rev. Lett. **85**, 2356 (2000).

<sup>14</sup> D. Loss and D. P. DiVincenzo, Phys. Rev. A **57**, 120 (1998).

<sup>15</sup> G. Burkard, D. Loss, and D. P. DiVincenzo Phys. Rev. B **59**, 2070 (1999).

<sup>16</sup> John Schliemann, Daniel Loss, and A. H. MacDonald, Phys. Rev. B **63**, 085311 (2001).

<sup>17</sup> V. W. Scarola and S. Das Sarma, Phys. Rev. A **71**, 032340 (2005).

<sup>18</sup> S. D. Lee, S. J. Kim, J. S. Kang, Y. B. Cho, J. B. Choi, Sooa Park, S.-R. Eric Yang, S. J. Lee, T. H. Zyung, cond-mat/0410044.

<sup>19</sup> A. K. Hüttel, S. Ludwig, H. Lorenz, K. Eberl, and J. P. Kotthaus, Phys. Rev. B **72** 081310(R) (2005).

<sup>20</sup> J. M. Elzerman, R. Hanson, J. S. Greidanus, L. H. Willems van Beveren, S. De Franceschi, L. M. K. Vandersypen, S. Tarucha, and L. P. Kouwenhoven, Phys. Rev. B **67**, 161308(R) (2003).

<sup>21</sup> A. C. Johnson, J. R. Petta, J. M. Taylor, A. Yacoby, M. D. Lukin, C. M. Marcus, M. P. Hanson, and A. C. Gossard, Nature **435**, 925 (2005).

<sup>22</sup> F. H. L. Koppens, J. A. Folk, J. M. Elzerman, R. Hanson, L. H. Willems van Beveren, I. T. Vink, H. P. Tranitz, W. Wegscheider, L. P. Kouwenhoven, and L. M. K. Vandersypen, Science **309**, 1346 (2005).

<sup>23</sup> J. M. Elzerman, R. Hanson, L. H. Willems van Beveren, B. Witkamp, L. M. K. Vandersypen, and L. P. Kouwenhoven, Nature **430**, 431 (2004).

<sup>24</sup> R. Hanson, L. H. Willems van Beveren, I. T. Vink, J. M. Elzerman, W. J. M. Naber, F. H. L. Koppens, L. P. Kouwenhoven, and L. M. K. Vandersypen, Phys. Rev. Lett. **94**, 196802 (2005).

<sup>25</sup> J. R. Petta, A. C. Johnson, J. M. Taylor, E. A. Laird, A. Yacoby, M. D. Lukin, C. M. Marcus, M. P. Hanson, and A. C. Gossard, Science **309**, 2180 (2005).

<sup>26</sup> E. Räsänen, A. Harju, M. J. Puska, and R. M. Nieminen, Phys. Rev. B **69**, 165309 (2004).

<sup>27</sup> P. S. Drouvelis, P. Schmelcher and F. K. Diakonos, J. of Phys.: Condens. Matter **16**, 3633 (2004).

<sup>28</sup> P. S. Drouvelis, P. Schmelcher and F. K. Diakonos, Phys. Rev. B **69**, 035333 (2004).

<sup>29</sup> P. S. Drouvelis, P. Schmelcher and F. K. Diakonos, Phys. Rev. B **69**, 155312 (2004).

<sup>30</sup> B. Szafran, F. M. Peeters, S. Bednarek, and J. Adamowski, Phys. Rev. B **69**, 125344 (2004).

<sup>31</sup> B. Szafran, F. M. Peeters, S. Bednarek, Phys. Rev. B **70**, 205318 (2004).

<sup>32</sup> B. Szafran and F. M. Peeters, Phys. Rev. B **71**, 245314 (2005).

<sup>33</sup> R. Ugajin, Physica B **253**, 92 (1998).

<sup>34</sup> T. H. Oosterkamp, S. F. Godijn, M. J. Uilenreef, Y. V. Nazarov, N. C. van der Vaart, and L. P. Kouwenhoven, Phys. Rev. Lett. **80**, 4951 (1998).

<sup>35</sup> M. P. Schwarz, D. Grundler, M. Wilde, C. Heyn, and D. Heitmann, J. Appl. Phys. **91**, 6875 (2002).

<sup>36</sup> M. P. Schwarz, D. Grundler, Ch. Heyn, D. Heitmann, D. Reuter, and A. Wieck, Phys. Rev. B **68**, 245315 (2003).

<sup>37</sup> P. A. Maksym and Tapash Chakraborty, Phys. Rev. B **45**, R1947 (1992).

<sup>38</sup> Weidong Sheng, and Hongqi Xu, Physica B **256-258**, 152 (1998).

<sup>39</sup> J. I. Climente, J. Planelles, and J. L. Movilla, Phys Rev. B **70**, 081301(R) (2004).

<sup>40</sup> I. Magnúsdóttir and V. Gudmundsson, Phys. Rev. B **61**, 10229 (2000).

<sup>41</sup> A. Aldea, V. Moldoveanu, M. Niță, A. Manolescu, V. Gudmundsson, and B. Tanatar, Phys. Rev. B **67**, 035324 (2003).

<sup>42</sup> H. Saarikoski, A. Harju, M. J. Puska, R. M. Nieminen, Phys. Rev. Lett. **93**, 116802 (2004).

<sup>43</sup> M. B. Tavernier, E. Anisimovas, and F. M. Peeters, Phys. Rev. B **70**, 155321 (2004).

<sup>44</sup> M. Toreblad, M. Borgh, M. Koskinen, M. Manninen, and S. M. Reimann Phys. Rev. Lett. **93**, 090407 (2004).

<sup>45</sup> H. Saarikoski, S. M. Reimann, E. Räsänen, A. Harju, and M. J. Puska, Phys. Rev. B **71**, 035421 (2005).

<sup>46</sup> H. Saarikoski and A. Harju, Phys. Rev. Lett. **94**, 246803 (2005).

<sup>47</sup> M. Marlo-Helle, A. Harju, and R. M. Nieminen, Physica E **26**, 286 (2005).

<sup>48</sup> H. A. Jahn and E. Teller, Proc. R. Soc. London A **161**, 220 (1937).

<sup>49</sup> J. K. Jain and T. Kawamura, Europhys. Lett. **29**, 321 (1995).

<sup>50</sup> A. Harju, B. Barbiellini, R. M. Nieminen, and V. A. Sverdlov, Physica B **255**, 145 (1998).